J|A|C|S
ARTICLES
Published on Web 01/08/2003

Mechanistic Studies on the Interaction of Reduced Cobalamin (Vitamin B_{12r}) with Nitroprusside

Maria Wolak,[†,‡] Grazyna Stochel,*[,†] and Rudi van Eldik*[,‡]

Faculty of Chemistry, Jagiellonian University, 30060 Krakow, Poland, and Institute for Inorganic Chemistry, University of Erlangen-Nürnberg, Egerlandstr. 1, 91058 Erlangen, Germany

Received August 14, 2002; E-mail: vaneldik@chemie.uni-erlangen.de

Abstract: The electron-transfer reaction between reduced cobalamin (Cbl(II)) and sodium pentacyanonitrosylferrate(II) (sodium nitroprusside, NP), as well as the subsequent processes following the electron-transfer step, were investigated by spectroscopic (UV−vis, ^{1}H NMR, EPR), electrochemical (CV, DPV) and kinetic (stopped-flow) techniques. In an effort to clarify the complex reaction pattern observed at physiological pH, systematic spectroscopic and kinetic studies were undertaken as a function of pH (1.8−9) and NP concentration (0.0001 − 0.09 M). The kinetics of the electron-transfer reaction was studied under pseudo-first-order conditions with respect to NP. The reaction occurs in two parallel paths of different order, viz. pseudo-first and pseudo-second order with respect to the NP concentration, respectively. The contribution of each path depends on pH and the [NP]/[Cbl(II)] ratio. At low pH and total NP concentration (pH < 3, [NP]/[Cbl(II)] ≈ 1), the cyano-bridged successor complex [Cbl(III)−(μ-NC)-$Fe^{I}(CN)_3(NO^+)]^-$ (**1**$_s$) is the final reaction product formed in an inner-sphere electron transfer reaction that is coupled to the release of cyanide from coordinated nitroprusside. At higher pH, subsequent reactions were observed which involve the attack of cyanide released in the electron transfer step on the initially formed cyano-bridged species, and lead to the formation of Cbl(III)CN and $[Fe^{I}(CN)_4(NO^+)]^{2-}$. The strong dependence of the rate and mechanism of the subsequent reactions on pH is attributed to the large variation in the effective nucleophilicity of the cyanide ligand in the studied pH range. An alternative electron-transfer pathway observed in the presence of excess NP involves the reaction of the precursor complex [Cbl(II)−(μ-NC)−$Fe^{II}(CN)_4(NO^+)]^{2-}$ (**1**$_p$) with NP to give [Cbl(III)−(μ-NC)−$Fe^{II}(CN)_4(NO^+)]^-$ (**2**) and reduced nitroprusside, $[Fe(CN)_5NO]^{3-}$, as the initial reaction products. Analysis of the kinetic data allowed elucidation of the rate constants for the inner- and outer-sphere electron-transfer pathways. The main factors which influence the kinetics and thermodynamics of the observed electron-transfer steps are discussed on the basis of the spectroscopic, kinetic and electrochemical results. A general picture of the reaction pathways that occur on a short (s) and long (min to h) time scale as a function of pH and relative reactant concentrations is derived from the experimental data. In addition, the release of NO resulting from the one-electron reduction of NP by Cbl(II) was monitored with the use of a sensitive NO electrode. The results obtained in the present study are discussed in reference to the possible influence of cobalamin on the pharmacological action of nitroprusside.

Introduction

Cobalamin (vitamin B_{12}, compare Figure 1) is a cobalt-containing macrocyclic complex, which serves as a cofactor in a number of cobalamin-dependent enzymatic processes. Equatorial positions in cobalamin are occupied by the corrin ring, which is structurally related to the porphyrin ligand. The axial position below the corrin ring (α site) is usually occupied by an intramolecularly bound 5,6-dimethylbenzimidazole group. The upper axial position (β site) in oxidized forms of cobalamin (containing a Co(III) center) can be occupied by different ligands (typically H_2O in aquacobalamin or CN^- in cyanocobalamin), whereas in the reduced form (containing a Co(II) center), the complex is five-coordinate, with one of the axial positions remaining vacant.

We have developed an interest in the reactions of the oxidized and reduced forms of cobalamin with NO[1,2] and selected NO-donating compounds that are of physiological and pharmacological importance. The purpose of these studies is to investigate and understand in more detail the specific interactions which could lead to the observed modification of the physiological activity of NO and selected NO-donors. Although several studies have indicated the possible biological significance of such interactions,[3−6] their chemical nature has not been

[†] Faculty of Chemistry, Jagiellonian University.
[‡] Institute for Inorganic Chemistry, University of Erlangen-Nürnberg.

(1) Wolak, M.; Stochel, G.; Hamza, M.; van Eldik, R. *Inorg. Chem.* **2000**, *39*, 2018.
(2) Wolak, M.; Zahl, A.; Schneppensieper, T.; Stochel, G.; van Eldik, R. *J. Am. Chem. Soc.* **2001**, *123*, 9780.
(3) Kruszyna, H.; Magyar, J. S.; Rochelle, L. G.; Russell, M. A.; Smith, R. P.; Wilcox, D. E.*J. Pharmacol. Exp. Ther.* **1998**, *285*, 665 and references therein.
(4) Brouwer, M.; Chamulitrat, W.; Ferruzzi, G.; Sauls, D. L.; Weinberg, J. B. *Blood* **1996**, *88*, 1857 and references therein.
(5) Zheng, D.; Birke, R. *J. Am. Chem. Soc.* **2001**, *123*, 4637 and references therein.

10.1021/ja0210852 CCC: $25.00

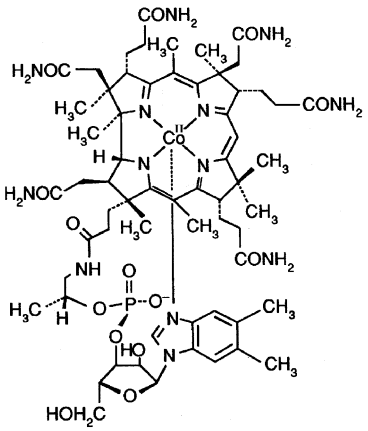

Figure 1. Molecular structure of reduced cobalamin, Cbl(II).

clarified. In our earlier studies, we reported on the kinetic and mechanistic characterization of the reaction between reduced cobalamin and NO. This reaction was shown to result in the formation of a stable Cbl(III)(NO^-) complex on a microsecond time scale,[2] and thus may contribute to the observed inhibition of the physiological activity of NO in the presence of cobalamin.

We now report spectroscopic and kinetic studies on the reaction of reduced cobalamin with a well recognized hypotensive agent sodium pentacyanonitrosylferrate(II), commonly known as sodium nitroprusside (SNP). The therapeutic properties of the nitroprusside ion, $[Fe(CN)_5NO]^{2-}$ (NP), depend on the release of nitric oxide, which in this formally Fe(III) nitrosyl is considered as a three electron donor (i.e., NO^+) bound to the low-spin Fe(II) center. Despite numerous studies on the chemical reactivity and electronic properties of nitroprusside, the mechanisms that lead to the observed physiological activity of this compound are not fully understood. Two possible pathways have been suggested in this context, the first of which relates mainly to the ability of $[Fe^{II}(CN)_5(NO^+)]^{2-}$ to act as an NO^+ donor in reactions with intracellular nucleophiles (most importantly thiols).[7] The other pathway of NO release is suggested to proceed via the redox conversion of NP to its one- or two-electron reduced forms by reductants present in mammalian cells (such as ascorbic acid or glutathione).[8,9]

An important limitation of the practical pharmacological application of NP results from the fact that its metabolic decomposition is accompanied by release of CN^-. In this respect, cobalamin which strongly binds cyanide to form a nontoxic Cbl(III)CN complex ($K_{Cbl(III)CN} = 1.2 \times 10^{14}\ M^{-1}$),[10] was suggested as a scavenger of cyanide released from metabolized NP. Subsequent studies provided evidence that the physiological action of NP is altered in the presence of cobalamin,[11,12] and this effect was ascribed to the formation of a stable binuclear complex [Cbl(III)−(μ-NC)-$Fe^{II}(CN)_4(NO^+)$]$^-$ **(2)**, (eq 1)[11]

$$[Cbl(III)(H_2O)]^+ + [Fe^{II}(CN)_5(NO^+)]^{2-} \overset{K_1}{\rightleftharpoons} [Cbl(III)-(\mu\text{-NC})-Fe^{II}(CN)_4(NO^+)]^- + H_2O \quad (1)$$
$$\textbf{(2)}$$

Consequently, the use of cobalamin as an antidote for potential cyanide poisoning induced by nitroprusside has been questioned. Although kinetic and spectroscopic investigations have already provided a rather detailed description of the mechanism and products of reaction 1,[11,13] an interesting aspect which concerns the change in redox activity of nitroprusside due to the formation of complex **2**, has not been elucidated and will be addressed in the present study. The main goal of the work presented here, however, was to investigate the intrinsic reactivity of reduced cobalamin, a cobalamin derivative occurring in vivo,[14] and sodium nitroprusside. We report on the formation and subsequent thermal reactions of the cyano-bridged complex [Cbl(II)−(μ-NC)−$Fe^{II}(CN)_4(NO^+)$]$^{2-}$ **(1_p)** (a one-electron reduced form of **2**), and comment on its possible biological relevance in relation to release of NO from $[Fe(CN)_5NO]^{2-}$.

A purely chemical aspect of this work is related to the chemistry of oligonuclear cyano-bridged M−CN−M′ complexes. Structural and electronic features as well as redox properties of such complexes have been extensively studied in recent years with respect to intermetallic electronic coupling, thermal and photoinduced electron transfer, and energy transfer processes occurring in such systems. Several examples of Co−(μ-NC)−Fe complexes have been prepared and examined in the context of electron-transfer processes.[11,13,15−17] These include recent studies on the $[(N)_5Co^{III}-(\mu\text{-NC})-Fe^{III}(CN)_5]^n$ and $[(N)_5Co^{II}-(\mu\text{-NC})-Fe^{III}(CN)_5]^{n-1}$ complexes, where $(N)_5$ denotes a pentadentate macrocyclic amine.[15,16] Spectroscopic and kinetic studies presented here concern the redox and substitution reactivity of the binuclear cyano-bridged complex formed between two biologically relevant species, viz. Cbl(II) and $[Fe(CN)_5NO]^{2-}$.

Experimental Section

Materials. Hydroxocobalamin hydrochloride (> 98%) and sodium nitroprusside (~99.0%) were obtained from Sigma. Other chemicals used throughout this study were of analytical reagent grade. Solutions were prepared from deionized (Millipore) water. Due to the marked oxygen sensitivity of Cbl(II) and reduced NP, all solutions were prepared and handled in the absence of O_2 with the use of Schlenk techniques. Oxygen-free nitrogen was used to deoxygenate the solutions.

Kinetic and Spectroscopic Measurements. UV−vis spectral changes and slow kinetic measurements were performed in gastight cuvettes in the thermostated (± 0.1 °C) cell compartment of a Shimadzu UV-2001 spectrophotometer. Faster spectral changes, as well as single-wavelength kinetic measurements, were recorded on an Applied

(6) Zheng, D.; Birke, R. *Inorg. Chem.* **2002**, *41*, 2548 and references therein.
(7) Oszajca, J.; Stochel, G.; Wasielewska, E.; Stasicka, Z.; Gryglewski, R. J.; Jakubowski, A.; Cieslik, K. *J. Inorg. Biochem.* **1988**, *69*, 121, and references therein.
(8) Wang, P. G.; Xian, M.; Tang, X.; Wu, X.; Wen, Z.; Cai, T.; Janczuk, A. J. *Chem. Rev.* **2002**, *102*, 1091, and references therein.
(9) (a) Smith, J. N.; Dasgupta, T. P. *Inorg. React. Mech.* **2002**, *3*, 181. (b) Smith, J. N.; Dasgupta, T. P. *J. Inorg. Biochem.* **2001**, *87*, 165, and references therein.
(10) Lexa, D.; Saveant, J. M.; Zickler, J. *J. Am. Chem. Soc.* **1980**, *102*, 2654.
(11) Butler, A. R.; Glidewell, C.; McIntosh, A. S.; Reed, D.; Sadler, I. H. *Inorg. Chem.* **1986**, *25*, 970 and references therein.
(12) (a) Li, C. G.; Rand, M. J. *Clin. Exp. Pharmacol. Physiol.* **1993**, *20*, 633. (b) Jenkinson, K. M.; Reid, J. J.; Rand, M. J. *Eur. J. Pharmacol.* **1995**, *275*, 145.
(13) Stochel, G.; van Eldik, R.; Kunkely, H.; Vogler, A. *Inorg. Chem.* **1989**, *28*, 4314.
(14) (a) Pezacka, E. H. *Biochim. Biophys. Acta* **1993**, *1157*, 167. (b) Watanabe, F.; Saido, H.; Yamaji, R.; Miyatake, K.; Isegawa, Y.; Ito, A.; Yobisui, T.; Rosenblatt, D. S.; Nakano, Y. *J. Nutr.* **1996**, *126*, 2947.
(15) (a) Bernhardt, P. V.; Martinez, M. *Inorg. Chem.* **1999**, *38*, 424. (b) Bernhardt, P. V.; Macpherson, B. P.; Martinez, M. *Inorg. Chem.* **2000**, *39*, 5203.
(16) Martinez, M.; Pitarque, M. A.; van Eldik, R. *Inorg. Chim. Acta* **1997**, *256*, 51.
(17) Rosenhein, L.; Speiser, D.; Haim, A. *Inorg. Chem.* **1974**, *13*, 1571.

Photophysics SX-17MV stopped-flow spectrophotometer equipped with a monochromator/PMT single wavelength detection system and a rapid scan J&M diode array detector. Kinetic and spectroscopic measurements were performed at 25 °C. Solutions of Cbl(II) were prepared by chemical reduction of aquacobalamin with sodium formate under inert atmosphere and subsequent dilution of the stock Cbl(II) solution with deoxygenated buffer to the appropriate concentration. Acetic acid/sodium acetate buffer (0.1 M) and Tris buffer (0.1 M, Sigma Chemicals; pH adjusted with $HClO_4$) were used to control pH in the range 4 to 5.5 and 7 to 9, respectively. Careful adjustment of the pH of Cbl(II) and NP solutions with deoxygenated $HClO_4$ or NaOH was done under other pH conditions. UV−vis/NIR spectra (200−3200 nm) of 1:1 Cbl(II)/NP mixtures (2×10^{-4} M) at pH 1.8 were recorded in acidified D_2O on a Cary 5000 spectrophotometer.

EPR measurements were performed at 120 K on a Bruker ESR 300 E spectrometer. Samples were prepared under inert atmosphere by addition of a molar equivalent of NP to the Cbl(II) solution (1×10^{-3} M) obtained by reduction of Cbl(II) with HCOONa in a 90% MeOH/10% H_2O mixture (pH of the Cbl(II) solution was carefully adjusted with small amounts of concentrated $HClO_4$ or NaOH prior to addition of NP). Aliquots of the samples were transferred in a gastight syringe to the evacuated quartz EPR sample tubes, rapidly frozen in liquid N_2 and sealed to prevent entry of air.

NMR spectra were recorded on a Bruker Avance DPX300 NB spectrometer operating at 300.13 MHz. Samples were prepared by chemical reduction of aquacobalamin (2×10^{-3} M) in deoxygenated D_2O followed by addition of 1 equiv of NP. The apparent pH (pH_{app} = pH meter reading = pD − 0.4) was adjusted by addition of DCl or NaOD prior to addition of NP, and carefully remeasured before transferring the solutions to gastight NMR tubes. Chemical shifts were referenced internally to trimethylsilyl propionate (TSP).

Electrochemical Measurements. Cyclic and differential pulse voltammograms were recorded using an EG&G Princeton Applied Research Model 263 potentiostat. All measurements were performed at room temperature under nitrogen atmosphere in a VC-2 voltammetry cell (Bioanalytical Systems) with a standard three-electrode configuration. Pt wire and a glassy carbon disk electrode (3.0 mm diameter) were used as counter and working electrodes, respectively. Due to the marked adsorption of the products of the electrochemical processes, the surface of the working electrode was polished with 0.05 μm alumina suspension prior to every scan. All potentials are referenced to an aqueous Ag/AgCl electrode ($E° = 0.222$ V). $NaClO_4$ solution (0.1 M) adjusted with NaOH or $HClO_4$ to the appropriate pH, or 0.1 M phosphate buffer was used as a supporting electrolyte.

NO Electrode Measurements. The release of NO resulting from the addition of Cbl(II) to NP was monitored with the Isolated Nitric Oxide Meter (WPI Instruments, model ISO−NO) calibrated by the standard chemical method described in the suppliers manual (generation of NO from $NaNO_2$ in the presence of excess KI at acidic pH). Measurements were performed in the dark under oxygen-free conditions.

Results and Discussion

Preliminary Observations. Preliminary UV−vis spectroscopic and kinetic observations showed that the reaction of cob(II)alamin with $[Fe(CN)_5NO]^{2-}$ is complex. The nature and rate of the overall process, as well as the observed intermediates and ultimate reaction products, strongly depended on pH, the relative concentrations of the reactants, and the nature of the solvent used as reaction medium. It was also evident from these observations that electron-transfer processes are operative in the studied system. It can on the basis of the redox potentials of the reacting species (−0.04 and −0.36 V vs Ag/AgCl for Cbl(III)/Cbl(II) and $[Fe(CN)_5NO]^{2-}/[Fe(CN)_5NO]^{3-}$, respectively at pH 7.4), be expected that the outer-sphere electron transfer between Cbl(II) and $[Fe(CN)_5NO]^{2-}$ is thermodynamically unfavorable, and the observed redox processes involve an inner-sphere electron-transfer mechanism. The primary reactions which should be considered include formation of the precursor cyano-bridged complex $[Cbl(II)-(\mu\text{-}NC)-Fe^{II}(CN)_4(NO^+)]^{2-}$ (**1**$_p$), the electron-transfer step, and subsequent reactions which lead to decomposition of the binuclear species. Indeed, these steps have been observed, and their occurrence and rate depended on the selected experimental conditions. The complicated reactivity pattern observed results from rather complex redox and substitution chemistry of both cobalamin and NP. This mainly includes the influence of the ligand environment on the redox properties of the Co and Fe centers present in cobalamin[18] and NP, respectively, as well as the observed instability of the initially formed reaction products toward substitution by cyanide present in the reaction medium.

Due to the biological relevance of the studied reaction, our first attempt was to perform spectroscopic and kinetic investigations of the observed redox process at physiological pH. These initial studies were frustrated by a complicated pattern of UV−vis spectral changes observed at this pH, from which the occurrence of reaction steps involving consecutive equilibration processes could be inferred. The absorbance changes resulting from these processes overlapped to a great extent, such that the identity and kinetic behavior of the individual species was difficult to resolve. These issues, however, could be addressed by a systematic analysis of reactivity patterns as a function of pH (1.8−9) and nitroprusside concentration (0.0001−0.09M).

The UV−vis spectral changes recorded for equimolar mixtures of the mononuclear complexes in the pH range 1.8 to 9, as well as additional spectroscopic and electrochemical measurements in aqueous and methanolic solutions, greatly assisted the resolution of the primary and secondary reaction steps which occur at equimolar concentrations of the reactants. With this information, it was then possible to interpret more complex spectral data and analyze kinetic results obtained in the presence of an excess of sodium nitroprusside, as described below.

Equimolar Concentrations of the Reactants. Spectroscopic Observations at Low pH. Successive additions of nitroprusside to a Cbl(II) solution at pH ≤ 2.5 under nitrogen atmosphere resulted in definite changes in the UV−vis spectrum of cobalamin,[19] with isosbestic points observed at 342, 385, and 495 nm, as presented in Figure 2. The plot of absorbance at 470 nm versus total NP concentration (inset in Figure 2) indicates a stoichiometry of close to 1:1 at equimolar concentrations of the reactants, and a high equilibrium constant ($K \gg 10^3$ M^{-1}) for the observed reaction. The spectral changes recorded with a diode-array detector on a stopped-flow instrument indicated that formation of the product is relatively rapid under the employed experimental conditions ($t_{1/2} < 1$ s). This product is stable under inert atmosphere, but in the presence of air is oxidized, giving a spectrum identical to that of [Cbl(III)−

(18) Lexa, D.; Saveant, J. M. *Acc. Chem. Res.* **1983**, *16*, 235 and references therein.

(19) Due to the strong absorption bands of the corrin ring in the UV−vis region, cobalamin is a much more distinctive chromophore compared to the nitroprusside ion. The intraligand electronic transitions of cobalamin are very sensitive to the oxidation state of the cobalt centre and nature of the ligands present in the axial positions. Consequently, UV−vis spectroscopy provides a good way to characterize the cobalamin reaction products, but not those of the cyanonitrosylferrate species.

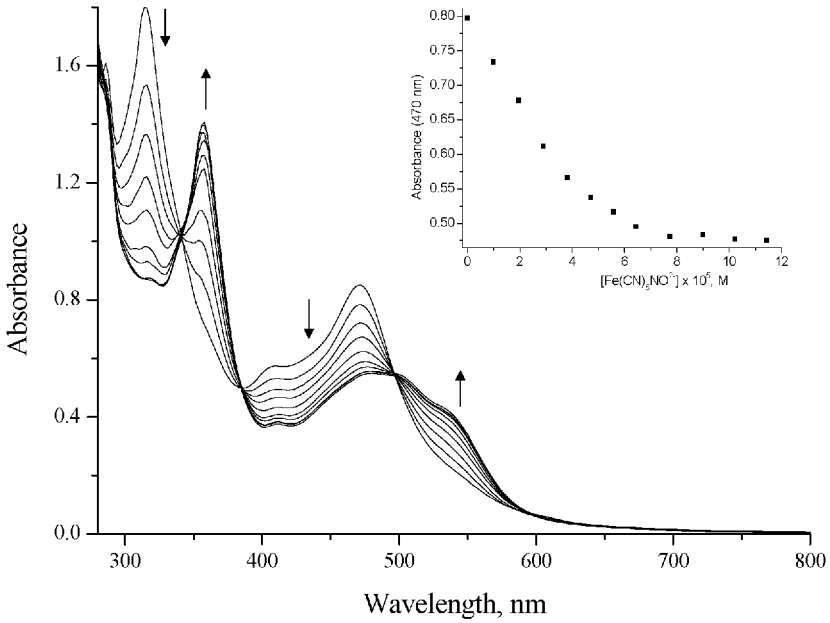

Figure 2. Spectral changes observed for the reaction of Cbl(II) (8×10^{-5} M) with NP at pH 2.5. Inset: plot of the absorbance at 470 nm versus total NP concentration.

Scheme 1

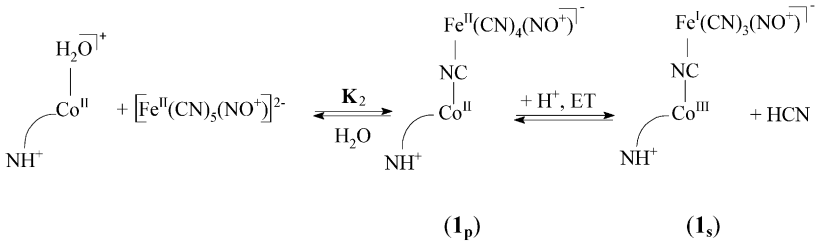

(μ-NC)−$Fe^{II}(CN)_4(NO^+)$]$^-$ (the spectral changes for this reaction exhibit well-defined isosbestic points at 290, 340, 370, and 498 nm).

A decrease in absorbance at 313 and 470 nm, accompanied by a significant absorbance increase at 352 and ca. 545 nm resulting from the addition of NP to Cbl(II), suggests a considerable shift of electron density away from the Co(II) center in the cobalamin product. However, the significant remaining absorbance at 313 and 480 nm, as well as the absence of the ^{1}H NMR spectrum (see NMR data presented below) and oxygen sensitivity of the product, indicate that the cobalt center partially retains its Co(II) character. Further evidence in support of this statement comes from EPR measurements. The EPR spectrum obtained after addition of NP to reduced cobalamin at pH 2 (Figure S1, Supporting Information) differs entirely from that of reduced cobalamin observed under similar experimental conditions.[20] A key feature of the spectrum is a strong EPR signal in the high field region, which is nearly identical with that observed for $[Fe^I(CN)_4(NO^+)]^{2-}$ formed after an one-electron reduction of NP in acidic medium. This signal is accompanied by a much weaker but clearly observable component that appears in the low-field range of the spectrum. The spectral features of this component resemble to some extent that exhibited by reduced cobalamin. In particular, a multi-line hyperfine splitting pattern was observed, which could be ascribed to the interaction of an unpaired electron with ^{57}Co. The hyperfine coupling constant of the low-field signal is significantly smaller than that observed for reduced cobalamin at pH 2 (ca. 150 G[20]). It is, however, similar to that observed in the $g_{||}$ component of Cbl(II) in the presence of cyanide (80 G[10,20]). Although detailed analysis of the spectrum was not performed, we conclude that the observed low-field component may reflect the residual unpaired electron density remaining on the cobalt center, as is also suggested by other spectroscopic data.

On the basis of the spectroscopic observations we ascribe the absorbance changes observed at low pH to the acid-catalyzed formation of the cyano-bridged binuclear species, [Cbl(III)−(μ-NC)−$Fe^I(CN)_3(NO^+)$]$^-$, (**1$_s$**). According to the reaction sequence presented in Scheme 1, the first step of the reaction involves coordination of NP to Cbl(II) which exists in this pH range in the base-off form.[18,21,22] Due to the high lability of the Co(II) center in reduced cobalamin, this step is expected to be very rapid. It was difficult to separate this step from the subsequent reactions under the employed experimental conditions. This could, however, be done for a model system involving the reaction of reduced cobalamin with $[Fe(CN)_6]^{4-}$. Addition of $[Fe(CN)_6]^{4-}$ to Cbl(II) solution results in a small but clearly observable change in the UV−vis spectrum of reduced cobalamin (Figure S3, Supporting Information). In this case, however, no subsequent electron transfer reactions occur,

(20) (a) Bayston, J. H.; Looney, F. D.; Pilbrow, J. R.; Winfield, M. E. *Biochemistry* **1970**, *9*, 2164. (b) Schrauzer, G. N.; Lee, L. P. *J. Am. Chem. Soc.* **1968**, *90*, 6541.

(21) Lexa, D.; Saveant, J. M.; Zickler, J. *J. Am. Chem. Soc.* **1977**, *99*, 2786.

such that the observed spectral changes can be unambiguously ascribed to formation of $[Cbl(II)-(\mu\text{-}NC)\text{-}Fe^{II}(CN)_5]^{4-}$ according to reaction 2

$$Cbl(II) + [Fe^{II}(CN)_6]^{4-} \overset{K_3}{\rightleftharpoons} [Cbl(II)-(\mu\text{-}NC)-Fe(CN)_5]^{4-} \quad (2)$$

Kinetic measurements showed that the rate of this process is too fast to be measured by stopped-flow technique. Detailed spectroscopic and kinetic measurements performed on the Cbl(II)/NP system (described in more detail below) indicate that formation of $\mathbf{1_p}$ results in a similar small spectral change and occurs on a time scale comparable to that observed for reaction 2.

Coordination of nitroprusside to Cbl(II) results in a very large negative shift in the redox potential of the cobalt center, such that it becomes significantly more negative than that characterizing the one-electron reduction of NP (electrochemical data supporting this statement are reported below). This change in potential provides the driving force for inner-sphere electron transfer within the binuclear complex. Oxidation of the cobalt center resulting from this process accounts for the substantial change in the UV−vis spectrum of reduced cobalamin. EPR spectra as well as other spectroscopic observations (see text below) indicated that the simultaneous one-electron reduction of the bound nitroprusside is accompanied by the release of HCN to the solution. The latter process can be ascribed to the release of cyanide from the trans position to the nitrosyl ligand in reduced nitroprusside (compare Scheme 1), in analogy to the well-known reaction observed for $[Fe(CN)_5NO]^{3-}$ at pH < 5[11,23−27]

$$[Fe^{II}(CN_{eq})_4(CN_{ax})(NO^{\bullet})]^{3-} + H^+ \rightleftharpoons [Fe^{I}(CN_{eq})_4(NO^+)]^{2-} + HCN \quad (3)$$

It should be noted that formation of $\mathbf{1_p}$ may involve coordination of nitroprusside through the cyanide located in the cis and trans position to the nitrosyl ligand, as was also observed for the reaction of $[Cbl(III)H_2O]^+$ with NP.[11] The release of cyanide from the cis isomer is expected to result in a rapid formation of $\mathbf{1_s}$, whereas in the case of the trans isomer, it would lead to decomposition of the precursor to Cbl(III)CN and $[Fe^{I}(CN_{eq})_4(NO^+)]^{2-}$. We conclude from the product distribution observed at low pH (see NMR data presented below) and from the statistics of the substitution process that the cis isomer is the main product of the substitution reaction outlined in Scheme 1.[28] Accordingly, $\mathbf{1_s}$ is the main reaction product observed in the studied system at low pH.

The postulated complex belongs to the class of oligonuclear M−NC−M′ species. A thoroughly investigated property of this class of compounds is the optically induced metal-to-metal charge-transfer giving rise to the intervalency band in their UV−vis−NIR spectra. Analysis of this optical transition according to the Hush theory often provides useful information on the thermodynamic free energy of the electron-transfer process, the center to center electronic coupling (H_{ab}), and the reorganizational energy (λ), which are related to the energy, intensity and halfwidth of the MMCT band, respectively. In the present case, no apparent peak which could be ascribed to a MMCT transition could be observed in the range 700−3200 nm. It is, however, possible, that this band is covered by the intense intraligand transitions of the equatorial cobalamin ligand, as was also suggested for the structurally related $[(N_5)Co^{III}-(\mu\text{-}NC)-Fe^{II}(CN)_5]^-$ dimers with pentadentate macrocyclic amine ligands.[15]

Spectroscopic Observations in the pH Range 3−9. The $[Cbl(III)-(\mu\text{-}NC)-Fe^{I}(CN)_3(NO^+)]^-$ complex is the long-lived species only in the lower pH range studied (pH < 3). On increasing pH, subsequent reactions leading to decomposition of the initially formed oligonuclear species were observed. In addition, significant changes occurred in the kinetics and thermodynamics of the inner-sphere electron-transfer step. The successive UV−vis spectral changes recorded for equimolar mixtures of the reactants in the pH range 2.4−9.0 indicated that the overall reaction proceeds via different pathways, the relative importance of which strongly depends on pH. This can be seen from a comparison of the time dependent spectral changes presented in Figure 3. The respective absorbance/time plots showing evolution of the absorbance at 540 nm reported in Figure 4 provide a semiquantitative kinetic characterization of primary and secondary reaction steps that occur at different pH. The following noteworthy features of the studied reaction can be concluded from these data.

1. The absorbance/time plots recorded within 50 s after mixing of the reactants at different pH (Figure 4a) indicate that the magnitude of the spectral change observed in this time domain (which directly reflects the inner-sphere electron transfer in $\mathbf{1_p}$) decreases on increasing pH. Consequently, the significant spectral change observed upon mixing of the reactants at pH 2 gradually decreases to a much less distinctive spectral change at higher pH (Figure 3c). The initial spectral change observed under these pH conditions (pH 5−8) resembles that resulting from the reaction of reduced cobalamin with $[Fe^{II}(CN)_6]^{4-}$ (i.e., formation of a cyano-bridged complex with a $Co^{II}-(\mu\text{-}NC)-Fe^{II}$ electronic configuration).

(22) Formation of the binuclear complex from base-off Cbl(II) may involve substitution of a very labile solvent molecule[2] by nitroprusside or its coordination at the vacant α position, thus leading to the formation of β- and α-substituted products, respectively. Indeed, the time-resolved UV−vis spectral changes and the respective absorbance/time plots obtained at pH ≤ 3 indicated the occurrence of two processes which exhibited a similar pattern of spectral changes (as shown in Figure S2, Supporting Information), but occurred at noticeably different rates. The contribution of the slower process to the overall reaction could be clearly observed at pH < 2, but became negligible at pH > 3, i.e., when the dimethylbenzimidazole ligand occupies the α position in Cbl(II). It is, therefore, reasonable to assume that the slower process reflects the formation and subsequent electronic stabilisation of the α-substituted cyano-bridged species. However, due to the fact that this reaction path occurs only at low pH and is of little relevance to the present study, its nature was not studied in more detail.

(23) (a) van Voorst, J. D. W.; Hemmerich, P. *J. Phys. Chem.* **1966**, *45*, 3914 and references therein. (b) Rao, D. N.; Cederbaum, A. I. *Biochim. Biophys. Acta* **1996**, *1289*, 195 and references therein.

(24) Cheney, R. P.; Simic, M. G.; Hoffman, M. Z. Taub, I. A. Asmus, K. D. *Inorg. Chem.* **1977**, *16*, 2187.

(25) Glidewell, C.; Johnson, I. L. *Inorg. Chim. Acta* **1987**, *132*, 145.

(26) Schwane, J. D.; Ashby, M. T. *J. Am. Chem. Soc.* **2002**, *124*, 6822.

(27) Gómez, J. A.; Guenzburger, D. *Chem. Phys.* **2000**, *253*, 73, and references therein.

(28) (a) NMR data reported in the literature suggest the formation of the trans isomer as the main product of the reaction between aquacobalamin and NP.[11] However, theoretical analyses of the charge distribution in $[Fe^{II}(CN)_5(NO^+)]^{2-}$ indicate similar net charges on the cyanide ligands located in the cis and trans position to NO,[27, 28b] with a slightly more negative charge for the cis cyanide (values such as −0.844 and −0.822 (au) were recently reported for the terminal nitrogen atoms in cis and trans cyanide, respectively[27]). This suggests similar nucleophilic reactivity of axial and equatorial cyanides toward coordination to the cobalt center, such that the product distribution will mainly be determined by the statistics of the substitution process. (b) Estrin, D. A.; Baraldo, L. M.; Slep, L. D.; Barja, B. C.; Olabe, J. A.; Paglieri, L.; Corongiu, G. *Inorg. Chem.* **1996**, *35*, 3897.

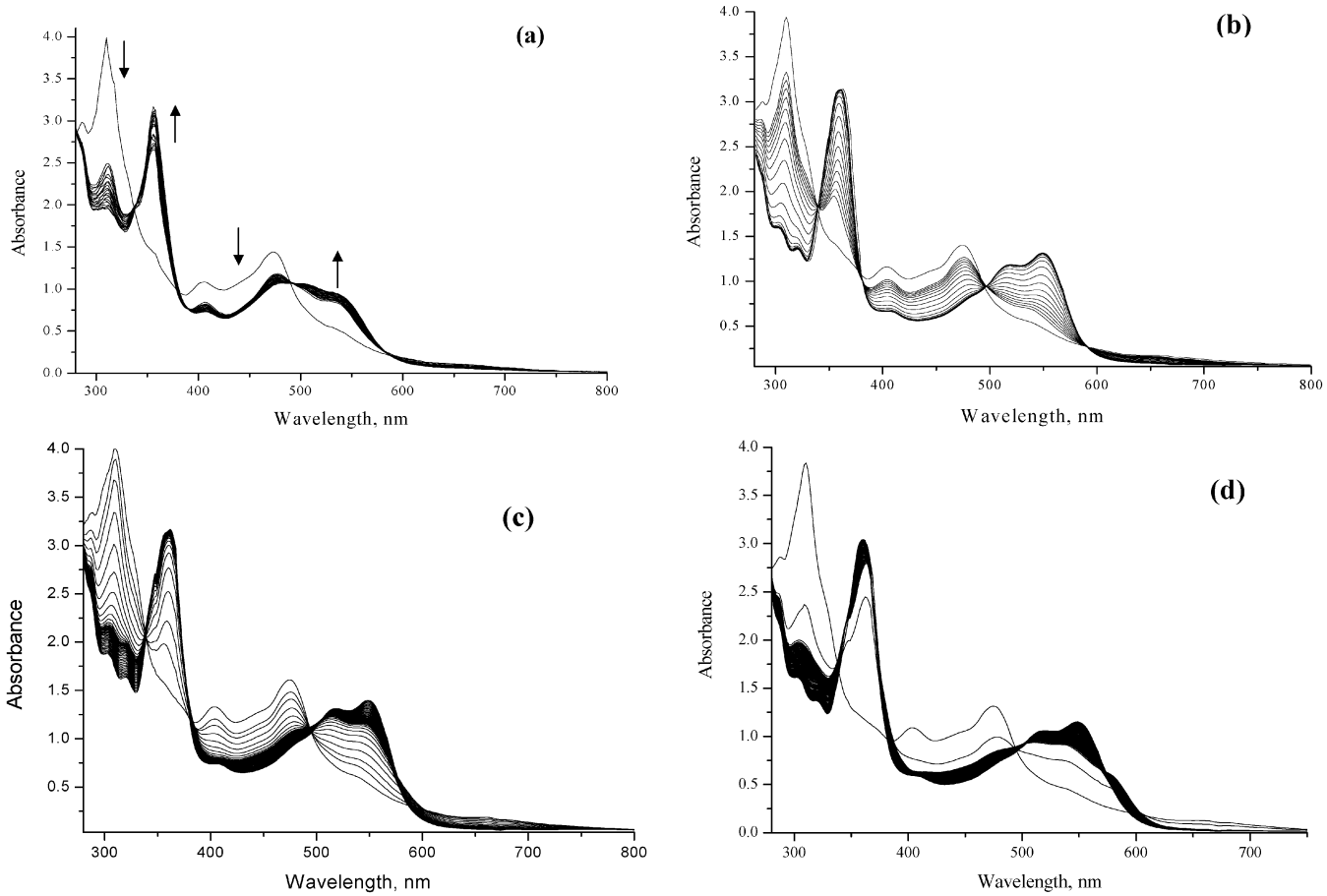

Figure 3. Time evolution of the UV−vis spectra for the reaction of Cbl(II) with NP at pH 3.3 (a), 5.5 (b), 7.4 (c) and 9.0 (d). Spectra recorded at time intervals of 1 min. [Cbl(II)] = [NP] = 2.5×10^{-4} M.

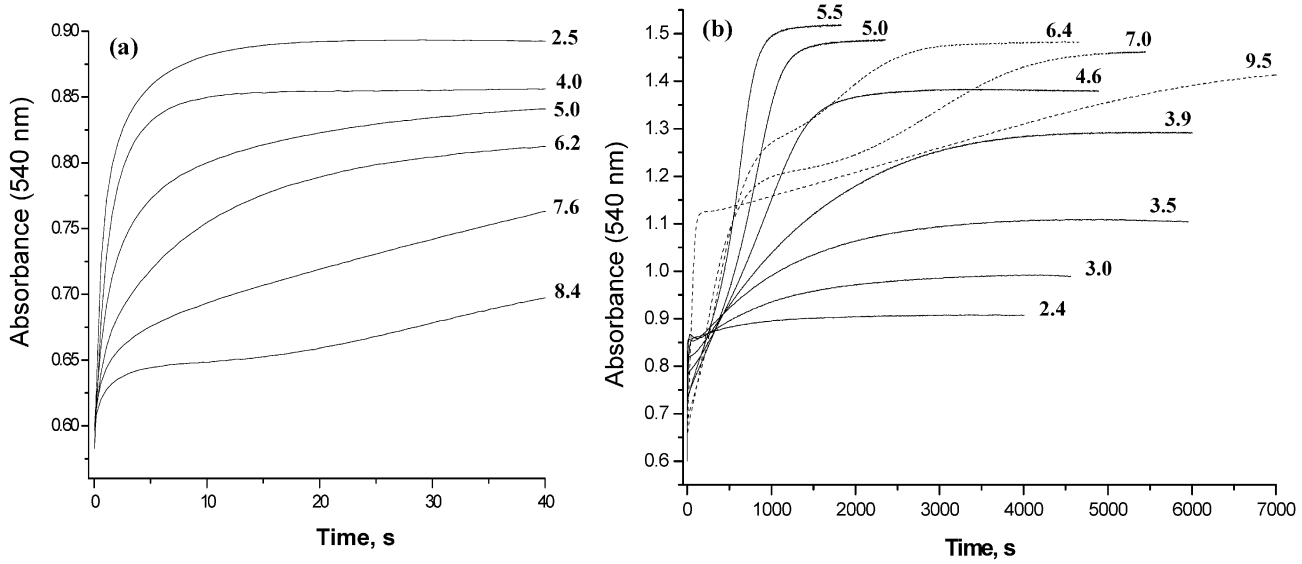

Figure 4. Absorbance/time plots showing the evolution of the absorbance at 540 nm over short (a) and long (b) time scale recorded for equimolar concentrations of Cbl(II) and NP (2.3×10^{-4} M) at different pH (indicated in the figure).

2. Data presented in Figures 3 and 4b show that at pH ≥ 3 the fast reaction steps are followed by subsequent reactions which occur on a longer time scale (min to h). The magnitude of the absorbance change resulting from these processes increases on increasing pH. Significant changes in absorbance at 313, 470, and 360 nm accompanied by the appearance of two bands centered at 515 and 547 nm observed during the slow reaction step, indicate conversion of the initially formed cyano-bridged species to a fully oxidized cobalamin product which could be identified as cyanocobalamin (Cbl(III)CN) on the basis of its UV−vis and ^{1}H NMR spectra. Figure 5 presents the aromatic region of the ^{1}H NMR spectra recorded as a

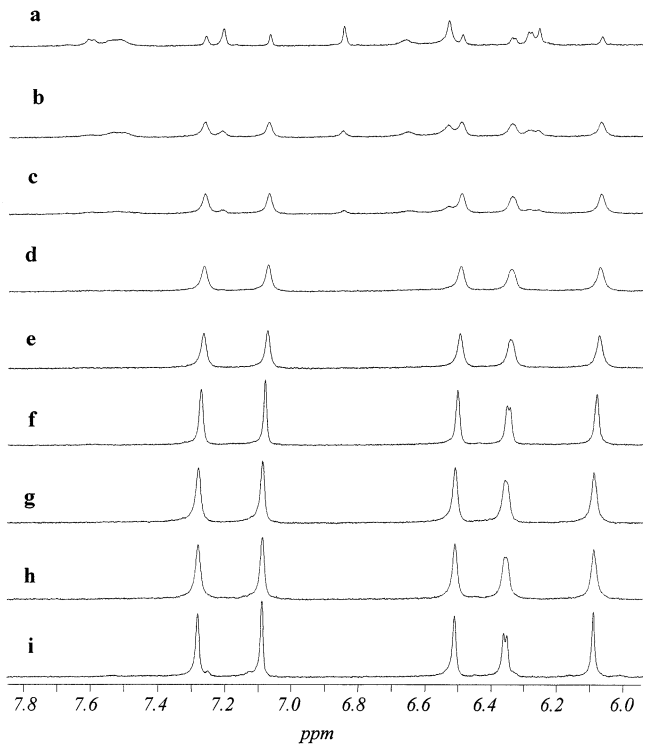

Figure 5. Aromatic region of the ^{1}H NMR spectra recorded after the reaction of equimolar concentrations of cob(II)alamin and NP (2×10^{-3} M) at pH_{app}: 2.0 (a), 3.1 (b), 3.5 (c), 4.0 (d), 4.5 (e), 5.1 (f), 5.5 (g), 6.0 (h), and 6.9 (i).

function of pH_{app} for equimolar mixtures of Cbl(II) and $[Fe(CN)_5NO]^{2-}$ ca. 3 h after mixing of the reactants. At $pH_{app} = 2$, weak signals attributable to small amounts of Cbl(III)CN and [Cbl(III)−(μ-NC)−$Fe^{II}(CN)_4(NO^+)$]$^-$ (**2**) were observed, the main cobalamin product being NMR silent.[29] On increasing pH, the intensity of the signals at 6.06, 6.28, 6.58, 7.14, and 7.26 ppm characteristic for Cbl(III)CN[30] increased, indicating a gradual increase in the conversion of the paramagnetic cobalamin species to cyanocobalamin.[31] NMR and UV−vis data indicated complete conversion of the cyano-bridged species to cyanocobalamin at pH > 5, whereas at lower pH an equilibrium mixture of $\mathbf{1_s}$ and Cbl(III)CN was observed.

3. Formation of cyanocobalamin in the final reaction step was preceded by characteristic induction periods which could be clearly distinguished from other reaction steps at pH > 4. EPR studies performed for equimolar Cbl(II) and $[Fe(CN)_5NO]^{2-}$ concentrations in a 90% MeOH/10% H_2O mixture at pH 7.4[32] indicated a decay of the Co(II) signal of cob(II)alamin and formation of a new signal characteristic for the $[Fe^I(CN)_4(NO^+)]^{2-}$ ion[23] during the induction period (compare Figure S4, Supporting Information). It follows that the induction periods directly reflect electron transfer between the cobalt and iron center at pH > 4. This process is apparently accompanied by the release of cyanide, as clearly evidenced by subsequent reactions involving the attack of cyanide on the initially formed cyano-bridged species.

4. The time evolution of the UV−vis spectra recorded at pH > 6 indicate an increasing contribution of a new reaction path which leads to the formation of Cbl(III)CN and $[Fe^I(CN)_4(NO^+)]^{2-}$ (as evidenced by UV−vis, ^{1}H NMR, and ERP spectroscopy) through intermediates different from that observed at lower pH. This can be seen on comparing the UV−vis spectra shown in Figure 3c and 3d, and the respective kinetic traces obtained at pH > 6 presented in Figure 4b. The characteristic pattern of UV−vis spectral changes featuring the additional reaction path, consisted of the appearance and subsequent slow decay of a shoulder in the range 560−600 nm. Occurrence of such a band in the low energy region of the spectrum indicates formation of cobalamin species in which the cyanide ion is coordinated at the α site of the corrin ring.[33] Formation of α-cyano substituted species could be clearly observed at physiological pH, and became the predominant reaction path at pH ≥ 8. Rapid scan measurements performed with a diode-array unit of a stopped-flow instrument allowed closer examination of this reaction path. The time evolution of the UV−vis spectra at pH 8.0 shown in Figure 6 allows resolution of two reaction steps within the time scale of the experiment (the final, third step occurs on a significantly longer time scale). The first step is evidenced by a characteristic initial spectral shift and subsequent small spectral changes observed as an induction period in the corresponding absorbance/time plot. We conclude on the basis of the UV−vis and EPR spectroscopic observations that this step involves formation of $\mathbf{1_p}$, followed by electron transfer and release of cyanide. These processes, however, occur initially in a rather small fraction of the precursor complex (see text below). The second reaction step that results in a large spectral change indicates quantitative conversion of the initially formed cyano-bridged species to the α-cyano substituted cobalamin. This process is characterized by isosbestic points at 390, 492, and 610 nm. The α-cyano substituted intermediate undergoes subsequent slow isomerization to cyanocobalamin, with isosbestic points at 576, 502, 370, 502, 370, 342, and 287 nm (compare Figure 3d). The rate of this process is strongly retarded on increasing pH, as evidenced by the final sections of the kinetic traces recorded at pH > 6 which are presented in Figure 4b.

Scheme 2 summarizes the main reactions suggested to account for the spectral evolution observed on a short (s) and long (min to h) time scale in the pH range 3−9.0. Due to the fact that reduced cobalamin exists in the base-on form at pH > 3,[18,21] formation of the precursor complex in this pH range involves rapid coordination of NP to the vacant β site of reduced cobalamin and is followed by inner-sphere electron transfer. Experimental results indicate, however, that the latter process is strongly influenced by the thermodynamics of cyanide release from the reduced nitroprusside moiety. In the case of free

(29) At pH 2 very weak signals were also observed at ca. 9.2, 7.6, 7.5, and 6.65 ppm. Although these signals clearly indicate formation of the base-off dimethylbenzimidazole-protonated cobalamin species, the low intensity and broad features of the signals do not allow their unambiguous assignment.

(30) Calafat, A.; Marzilli, L. *J. Am. Chem. Soc.* **1993**, *115*, 9182.

(31) Formation of $[Fe^I(CN)_4(NO^+)]^{2-}$ as the other reaction product was confirmed by EPR spectroscopy.

(32) (a) The UV−vis spectral changes and the respective absorbance/time plots recorded in this medium at different pH (adjusted with small amounts of NaOH or $HClO_4$), were in general similar to those observed for the reaction in water. The overall reaction time, however, and in particular the induction periods preceding the formation of cyanocobalamin, were significantly longer, such that this reaction step could be conveniently studied by conventional EPR spectroscopy. Significant deceleration of the reaction observed in methanolic medium can at least in part be ascribed to a decrease in driving force for the electron-transfer reaction due to a negative shift of the redox potential of the iron center on going from water to methanol.[32b] (b) Baraldo, L. M.; Forlano, P.; Parise, A. J.; Slep, L. D.; Olabe, J. A. *Coord. Chem. Rev.* **2001**, *219*, 881 and references therein.

(33) Hamza, M. S.; Zou, X.; Brown, K. L.; van Eldik, R. *Inorg. Chem.* **2001**, *40*, 5440, and references therein.

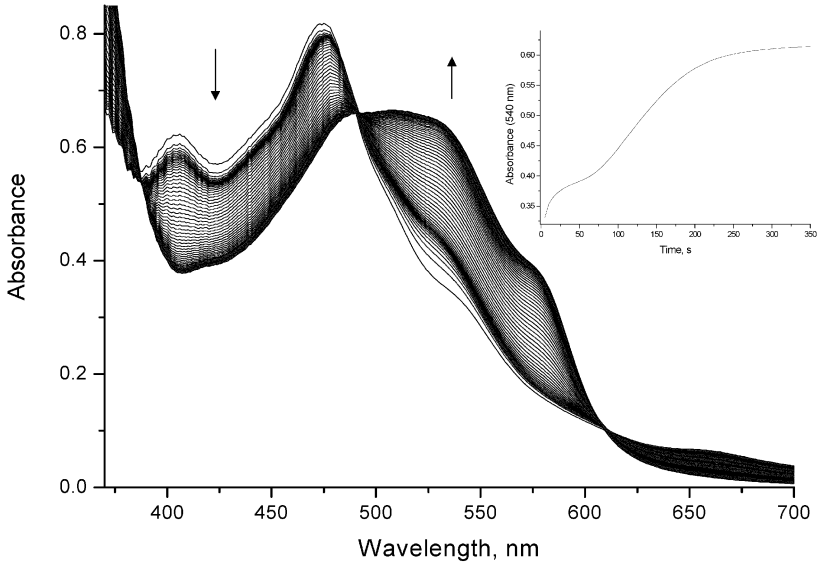

Figure 6. Time evolution of the UV−vis spectra recorded at time intervals of 5 s for an equimolar mixture of the reactants at pH 8.0. Experimental conditions: [Cbl(II)] = [NP] = 1×10^{-4} M, pH adjusted with NaOH. Inset: absorbance/time plot showing the evolution of absorbance at 540 nm.

Scheme 2

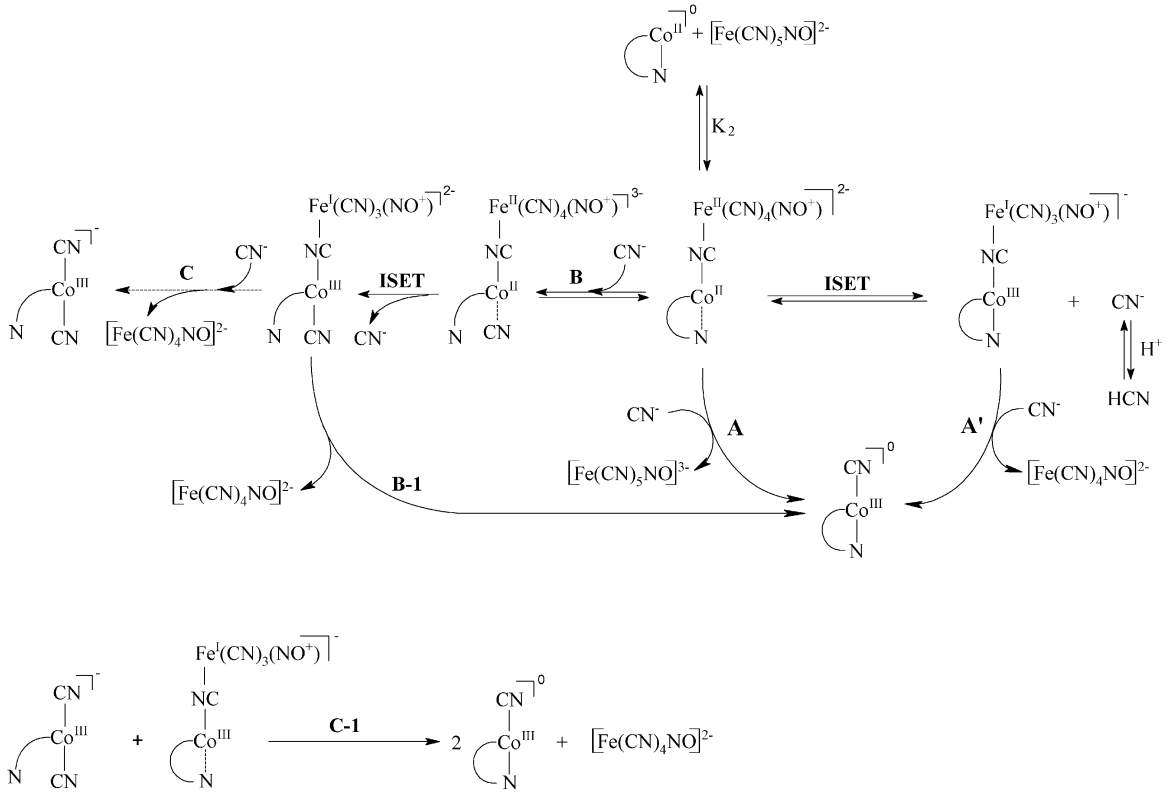

$[Fe(CN)_5NO]^{3-}$ ion, the following kinetic and thermodynamic parameters that characterize the release of cyanide (reaction 4) have been reported[24]

$$[Fe^{II}(CN)_5(NO^{\bullet})]^{3-} \underset{k_{-4}}{\overset{k_4}{\rightleftharpoons}} [Fe^{I}(CN)_4(NO^{+})]^{2-} + CN^- \quad K_4 = k_4/k_{-4} \qquad (4)$$

$$CN^- + H^+ \rightleftharpoons HCN$$

$k_4 = 2.8 \times 10^2\ s^{-1}$, $k_{-4} = 4 \times 10^6\ M^{-1}\ s^{-1}$ and $K_4 = 6.8 \times 10^{-5}$ M at 25 °C. Despite the small value of K_4, equilibrium (4) is shifted to the right at pH < 4 due to protonation of cyanide ($pK_a^{HCN} = 9.3 \pm 0.2$[24]). At pH > 6, however, the release of CN^- becomes thermodynamically unfavorable, such that $[Fe(CN)_5NO]^{3-}$ becomes the dominant form of reduced nitroprusside at basic pH. The p*K* values for the overall protonation equilibrium (5), determined by different experimental techniques, fall in the range 4.7−6.5[23,24,34]

$$[Fe^{II}(CN)_5(NO^{\bullet})]^{3-} + H^+ \rightleftharpoons [Fe^{I}(CN)_4(NO^{+})]^{2-} + HCN \qquad (5)$$

In the presently studied system, much slower reaction rates were observed for the electron-transfer coupled release of cyanide from $\mathbf{1_p}$ over the whole pH range studied, as compared to that

reported for $[Fe(CN)_5NO]^{3-}$. This emphasizes the different nature of the rate-determining step that leads to the loss of cyanide from bound and free reduced NP, as discussed in more detail below.

The reactivity of the cyano-bridged complex formed at pH > 5 involves spontaneous rather than proton-driven release of CN^-,[24] a process which is expected to be thermodynamically unfavorable (compare small value of K_4 for $[Fe(CN)_5NO]^{3-}$, reaction 4). Experimental data indicate that the thermodynamics of cyanide loss strongly affects inner-sphere electron transfer in the $[Cbl(II)-(\mu\text{-}NC)-Fe^{II}(CN)_4(NO^+)]^{2-}$ complex. The latter apparently becomes thermodynamically less favored at pH > 5, in comparison to that accompanying the proton-driven[24,34] release of cyanide at lower pH. In this context, the decrease in the initial absorbance change (Figure 4a) can be traced to the pH dependent equilibrium (6) determining the ratio of the $\mathbf{1_p}$ and $\mathbf{1_s}$ species, which gradually shifts to the right on decreasing pH

$$[Cbl(II)-(\mu\text{-}NC)-Fe^{II}(CN)_4(NO^+)]^{2-} + H^+ \rightleftharpoons [Cbl(III)-(\mu\text{-}NC)-Fe^{I}(CN)_3(NO^+)]^- + HCN \quad (6)$$

We conclude that the small initial change in absorbance observed after mixing of the reactants at pH > 7 reflects formation of the precursor complex $\mathbf{1_p}$ as the *main* initial reaction product, with little contribution from electron transfer to the absorbance change. From the magnitude of the initial spectral change observed at 540 nm, an apparent p*K* value of 5.7 was estimated for the overall protonation equilibrium (6) (compare data presented in Figure S5, Supporting Information). This value lies in the range of p*K* values reported for equilibrium (5), indicating that acid−base properties of nitroprusside in $[Cbl(II)-(\mu\text{-}NC)-Fe^{II}(CN)_4(NO^+)]^{2-}$ are not significantly different from that observed for $[Fe(CN)_5NO]^{3-}$.

The important influence of the release of cyanide on inner-sphere electron transfer observed in the present system was directly confirmed by an experiment in which equimolar concentrations of Cbl(II) and $[Fe(CN)_5NO]^{2-}$ (1×10^{-4} M) were reacted in the presence of Ag^+ ions ($[Ag^+] = 2 \times 10^{-4}$ M) at pH 7.4. The resulting spectral changes presented in Figure 7 closely resemble those observed at pH 2, and indicate rapid ($t < 0.2$ s) occurrence of inner-sphere electron transfer. This observation can be accounted for by rapid formation of $\mathbf{1_s}$ as outlined in Scheme 3.

Recent studies on the electron-transfer process involving reduction of NP by selected biological reductants indicated a similar strong influence of a reversible cyanide release on the thermodynamics of the electron-transfer reaction.[9]

The effect of the release of the peripheral cyanide ligand on the reducibility of the iron center in $\mathbf{1_p}$ can be rationalized in terms of large differences in the electronic structure of the $[Fe(CN)_5NO]^{3-}$ and $[Fe(CN)_4NO]^{2-}$ ions.[27] It has been reported that cyanide loss from $[Fe(CN)_5NO]^{3-}$ results in a drastic change in its electronic configuration. In particular, the nature of the SOMO orbital changes from that consisting primarily of the π^* orbital of NO (and to a lesser extent of the $3d_{xz}$ and $3d_{yz}$ orbitals of Fe) and exhibiting π symmetry, to one of σ symmetry in which the unpaired electron is localized mainly on the $3d_{z^2}$ orbital of Fe.[27] Similarities in the electrochemical properties of bound and free nitroprusside (as indicated by electrochemical data reported later in the text) imply that cyanide loss from $\mathbf{1_p}$ will result in analogous changes in the energy and symmetry of the HOMO orbital at the iron center. Such changes, however, may strongly modify the bridge-mediated metal−metal interactions which govern the inner-sphere electron-transfer process. Theoretical data on the electronic configuration of reduced nitroprusside outlined above suggest that cyanide release influences reducibility of the iron center by enabling the facile *iron-centered* reduction within the binuclear complex (electron transfer in the $Co^{II}-(\mu\text{-}NC)-Fe^{II}$ complex which does not release CN^- would be expected to result in a *ligand (NO)* rather than a *metal-centered* reduction of nitroprusside).

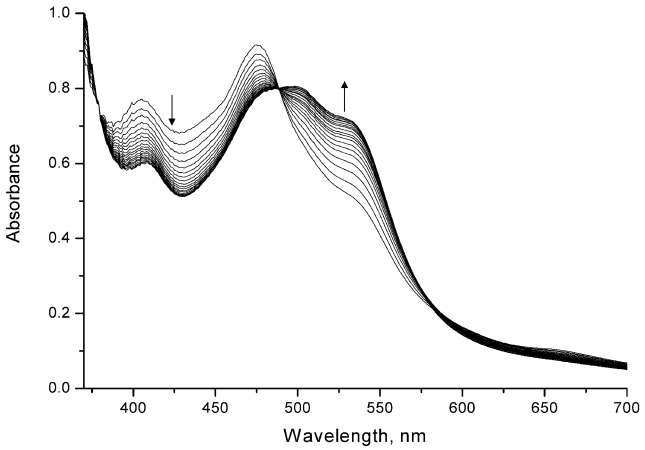

Figure 7. Time evolution of the UV−vis spectra recorded at pH 7.4 for an equimolar mixture of the reactants, $[Cbl(II)] = [NP] = 1 \times 10^{-4}$ M, in the presence of Ag^+ (2×10^{-4} M). Spectra recorded at time intervals of 0.01 s, overall reaction time 0.2 s; pH adjusted with Tris-$HClO_4$ buffer solution.

Scheme 3

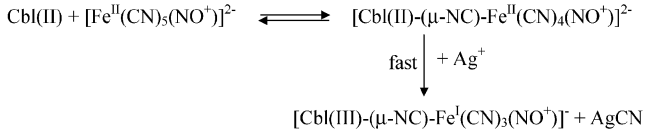

The subsequent slow reactions observed at pH > 3 result from the attack of cyanide liberated in the electron-transfer step, on the initially formed cyano-bridged species. This may occur along two reaction pathways involving the attack of CN^- on the β- or α-site of cobalamin, respectively. The relative contribution of both these pathways was observed to depend strongly on pH. Clean conversion of the cyano-bridged species to cyanocobalamin observed as the final reaction step in the pH range 3−6 can be accounted for by the reaction paths **A** and **A′** depicted in Scheme 2. Attack of cyanide on the upper (β) position of cobalamin in the cyano-bridged complexes $\mathbf{1_p}$ (path **A**) and/or $\mathbf{1_s}$ **(**path **A′)** leads to formation of a very stable Cbl(III)CN complex and thus, strong stabilization of the 3+ oxidation state of the cobalt center. The significant increase in the rate and degree of conversion of the cyano-bridged species to cyanocobalamin on increasing pH apparently reflects the increase in reactivity of the CN^- ions toward substitution. The observed induction periods preceding formation of cyanocobalamin indicate that cyanide ions, once released from the cyano-bridged species, accelerate the electron-transfer step.

(34) Masek, J.; Maslova, E. *Collect. Czech. Chem. Commun.* **1974**, *39*, 2141 and references therein.

Formation of the α-cyano intermediate observed at pH > 6 can be accounted for by a contribution of reaction path **B** which involves attack of cyanide at the α-position of cobalamin in [Cbl(II)−(μ-NC)−$Fe^{II}(CN)_4(NO^+)$]$^{2-}$ (**1p**). It is, in principle, possible that the α-cyano intermediate could be also formed via attack of CN^- at the α-position in the successor [Cbl(III)−(μ-NC)−$Fe^{I}(CN)_3(NO^+)$]$^-$ complex (**1s**). Very low concentrations of CN^- present under the employed experimental conditions imply, however, that the observed substitution of α-dimethylbenzimidazole can only occur if the Co−N(dimethylbenzimidazole) bond is very labile. It can be expected that the stabilization of the 3+ oxidation state of the cobalt center in **1s** would result in a stronger Co−N(dimethylbenzimidazole) bond[35] compared to that observed in **1p** (containing the labile Co(II) center). For this reason, the latter species is expected to be more reactive toward substitution at the α-position.

Attempts to characterize the α-cyano substituted intermediate by recording ^{1}H NMR spectra of the reaction mixture in basic D_2O, were not successful due to a relatively rapid conversion of the intermediates to cyanocobalamin under the experimental conditions employed in the NMR measurements (pD = 9.0, [Cbl(II)] = [$Fe(CN)_5NO^{2-}$] = 2×10^{-3} M). It was, however, possible to obtain such data when the reaction was carried out in CD_3OD at pD = 9[36] (adjusted with small amounts of NaOD). The aromatic region of the ^{1}H NMR spectrum recorded during the entire course of the reaction (data not shown) exhibited five intense peaks located at 7.25, 7.14, 6.58, 6.28(d), and 6.05 ppm, which are attributed to cyanocobalamin formed as the final cobalamin product (this was confirmed by recording the spectrum of an authentic sample of cyanocobalamin in CD_3OD at pH 9). In addition, five peaks of lower intensity and significantly broadened features were observed at 8.34, 7.41, 7.38, 6.31, and 5.79 ppm, i.e., at the positions almost identical with that observed for dicyanocobalamin, $Cbl(CN)_2$, (peaks at 8.36, 7.42, 7.38, 6.31, and 5.79 ppm, respectively) under the same experimental conditions. This result confirms coordination of the cyanide ligand at the α-site of cyanocobalamin in the observed intermediate. However, due to the fact that the ^{1}H NMR spectrum of the α-cyano substituted complex [(CN)Cbl(III)−(μ-NC)−$Fe^{I}(CN)_3(NO^+)$]$^{2-}$ can be similar to that of dicyanocobalamin (and in addition, is likely to exhibit significantly broadened peaks, as was indeed observed in the performed experiment), an unambiguous differentiation between these two species could not be made. Because the concentrations of CN^- liberated in the electron-transfer step are very low, formation of the mono-cyanide substituted [(CN)Cbl(III)−(μ-NC)−$Fe^{I}(CN)_3(NO^+)$]$^{2-}$ species rather than dicyanocobalamin is a reasonable indirect conclusion. However, the trans-labilizing effect of the cyanide ligand in the α−position may induce rapid displacement of [$Fe^{I}(CN)_4(NO^+)$]$^{2-}$ by a second CN^-, thus leading to the formation of dicyanocobalamin, as suggested in path **C** of Scheme 2. A similar reactivity pattern has indeed been observed for several organocorrinoids which undergo dealkylation by cyanide in a single kinetic step to give $Cbl(CN)_2$.[33] Irrespective of the exact nature of the α-cyano substituted intermediate, its decomposition in a final, slow reaction step observed at pH > 6 clearly involves the displacement of [$Fe^{I}(CN)_4(NO^+)$]$^{2-}$ coordinated to the cobalt center by CN^- released from the α-position of cobalamin, resulting in formation of Cbl(III)CN and [$Fe^{I}(CN)_4(NO^+)$]$^{2-}$ as the ultimate reaction products. Two possible pathways (**B-1** and **C-1**, Scheme 2) can be postulated for this process, depending on the actual nature of the α-cyano intermediate.

Literature data indicate that the cyanide ligand offers a greater stabilization of the 3+ oxidation state of the cobalt center in cobalamin compared to dimethylbenzimidazole.[10,18] Thus, substitution of the DMBI ligand by CN^- upon formation of the α-cyano intermediate is expected to promote electronic isomerization of **1p,** which in turn is coupled to the release of cyanide (as shown in the reaction path **B)**. The suggested reaction sequence offers a further mechanistic interpretation of cyanide-assisted inner-sphere electron transfer observed at high pH.

In the context of the reaction mechanism outlined in Scheme 2, the UV−vis spectral changes observed at physiological pH indicate rapid formation of a mixture of [Cbl(III)−(μ-NC)−$Fe^{I}(CN)_3(NO^+)$]$^-$ and [Cbl(II)−(μ-NC)−$Fe^{II}(CN)_4(NO^+)$]$^{2-}$ (**1p** and **1s**, respectively) in which the latter is the main initial product. The subsequent, slow reactions occurring at this pH mainly involve reactions **A** and **A′,** with a minor contribution of reaction sequence **B** to the overall process.

Excess of Nitroprusside. Spectroscopic Observations. To investigate in more detail the kinetics and mechanism of the observed electron-transfer process, kinetic studies under pseudo-first-order conditions with respect to nitroprusside were undertaken. The choice of the reactant used in excess was dictated by the need to avoid experimental complications which arose in the preliminary kinetic studies in the presence of excess Cbl(II).[37]

In analogy to the data obtained for equimolar concentrations of the reactants, spectroscopic observations in an excess of NP indicated the occurrence of fast and slow reaction steps, the nature and rate of which strongly depended on pH. However, the reactivity patterns were different from that observed under 1:1 stoichiometric conditions. In particular, a significant increase in the rate and in the degree of conversion of Cbl(II) to its oxidized form in the initial, fast reaction steps was observed on increasing the NP concentration. This is evidenced by the initial sections (0−400 s) of the absorbance/time plots presented in Figure 8. Spectroscopic data also indicated that [Cbl(III)−(μ-NC)−$Fe^{II}(CN)_4(NO^+)$]$^{2-}$ (**2**) rather than its reduced forms **1p** and **1s**, is the main cobalamin product formed in the electron-transfer step in the presence of excess NP. This observation can be accounted for by the reactions outlined in Scheme 4.

The reaction route characterized by the rate constant k_6 represents the contribution of outer-sphere electron transfer between **1p** and NP, to the overall process. Examination of the products formed in the electron-transfer step as a function of pH and NP concentration indicated that, in general, the

(35) Significantly stronger Co−N(DMBI) bond in typical Cbl(III) derivatives compared to Cbl(II) is evidenced by (i) shorter length of the Co−N(DMBI) bond (1.925 Å in [Cbl(III)H_2O]$^+$ [35b] compared to 2.13 Å in Cbl(II)[35c]), (ii) significantly lower pK_a values for deprotonation of the DMBI ligand[35d−e] (pK_a = −2.1 in [Cbl(III)H_2O]$^+$ compared to pK_a = 2.9 in Cbl(II)). (b) Kratky, C.; Farber, G.; Gruber, G.; Wilson, K.; Dauter, Z.; Nolting, H.-F.; Konrad, R.; Krautler, B. *J. Am. Chem. Soc.* **1995**, *117*, 4654. (c) Krautler, B.; Keller, W.; Kratky, C. *J. Am. Chem. Soc.* **1989**, *111*, 8936. (d) Brown, K. L. *J. Am. Chem. Soc.* **1987**, *26*, 2034 and references therein. (e) Brown, K. L.; Peck-Siler, S. *Inorg. Chem.* **1988**, *27*, 3548.

(36) Despite a significantly slower rate of the reaction compared to that observed in H_2O, formation of the α-cyano substituted species in CD_3OD was confirmed by a characteristic increase in absorbance in the range 580−600 nm of the UV−vis spectrum.

(37) These mainly include the high extinction coefficients of Cbl(II), and formation of cyano-bridged polynuclear species, such as Co−Fe−Co trimers.

Scheme 4

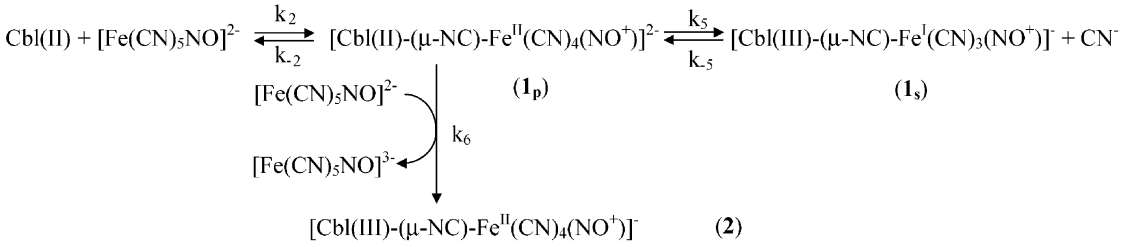

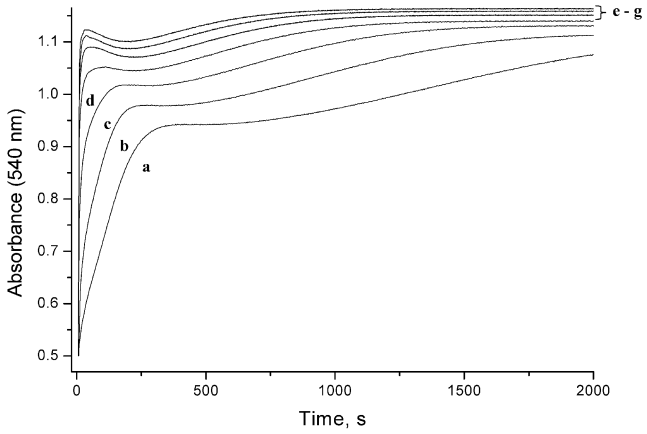

Figure 8. Absorbance/time plots recorded at pH 7.4 for the reaction of Cbl(II) (2×10^{-4} M) with an excess of NP. Concentrations of NP: 4 (a), 8 (b), 16 (c), 30 (d), 60 (e), 100 (f), and 150×10^{-4} M (g).

contribution of inner-sphere electron transfer is significant under conditions where [NP]/[Cbl(II)] $\leq$ 5, whereas at higher NP concentrations the outer-sphere pathway leading to formation of **2**, plays a dominant role (the relative contributions of both reaction routes at a given NP concentration also depended on pH, as discussed in more detail below).

Careful examination of the spectral changes that occur on a long time scale (100−2000 s) and a comparison with the respective slow spectral changes observed for equimolar concentrations of the reactants, enabled elucidation of the nature of the slow reaction steps, which in the presence of ca. 10 times (and higher) excess of sodium nitroprusside ([NP] > 0.001 M) occur only at pH > 5. It may be concluded from these studies that the subsequent reaction observed in the pH range 5−7 mainly involves substitution of nitroprusside in complex **2** (formed as the dominant initial reaction product) by cyanide, as shown in reaction 7

$$[\text{Cbl(III)}-(\mu\text{-NC})-\text{Fe}^{\text{II}}(\text{CN})_4(\text{NO}^+)]^- + \text{CN}^- \rightleftarrows \text{Cbl(III)CN} + [\text{Fe}^{\text{II}}(\text{CN})_5(\text{NO}^+)]^{2-} \quad (7)$$

A comparison of the stability constant reported for Cbl(III)CN (1.2×10^{14} M^{-1}) with that determined for complex **2** ($K_1 = 5 \times 10^6$ M^{-1}),[38] shows that reaction 7 is indeed thermodynamically favored. On further increasing pH, formation of the α-cyano substituted species could be observed, as evidenced by the emergence of a characteristic shoulder in the UV−vis spectrum at ca. 600 nm (this process was also accompanied by a decrease in absorbance at 540 nm following the initial rapid absorbance increase, compare the kinetic traces d−g reported in Figure 8). The contribution of this reaction path to the overall process was only small at physiological pH, but became significant at pH $\geq$ 8. Spectral changes observed under these pH conditions indicated that the cyanide-assisted electron-transfer processes involving formation of the α-cyano substituted intermediate (Scheme 2, reaction path **B**) are fast, and efficiently compete with the outer-sphere electron-transfer reaction. The final reaction step observed under neutral and basic pH conditions (reflected by the increase in absorbance at 540 nm in the final sections of the absorbance/time plots shown in Figure 8) indicate slow conversion of the α-cyano intermediate to cyanocobalamin. This process is expected to occur according to the same reaction mechanism as that suggested in Scheme 2 for 1:1 stoichiometric conditions.

Kinetic Measurements. Kinetics of the electron-transfer processes was studied by following the increase in absorbance in the UV−vis spectrum of reduced cobalamin at 530 nm. Under pseudo-first-order conditions with respect to NP, the electron-transfer step occurred within the time scale 0.05−5 s, depending on the selected experimental conditions. The kinetic traces obtained in the pH range 1.8−6 gave best mathematical fits to a kinetic model involving two first-order reactions. Analysis of the data with a two-exponential function indicated that the rate of both the slow and fast component increased on increasing pH and nitroprusside concentration. However, at a given pH value, the absorbance change resulting from the faster reaction increased on increasing the NP concentration, whereas that attributable to the slower component progressively decreased, and could no longer be observed at higher [NP]. The concentration of NP at which the contribution of the slower component became negligible decreased from ca. 0.06 M at pH 1.8 to ca. 0.006 M at pH 5. At pH > 5 the contribution of the slower component to the overall absorbance change could not be observed even at the lowest NP concentrations required to maintain pseudo-first-order conditions (0.001 M).

Experimental results clearly indicated that the two processes observed at pH $\leq$ 5 occur on a relatively similar time scale, such that the rate constants obtained for the slow and fast components differed by a factor $\leq$ 5. Consequently, although the general reactivity trends described above were evident from two-exponential analysis of kinetic traces, clear differentiation between the faster and the slower component was difficult, particularly when the amplitude attributable to one of the components was small. This resulted in a considerable scatter of the $k_{obs}(1)$ and $k_{obs}(2)$ values (ascribed to the faster and slower reaction, respectively) obtained from the two-exponential analysis (plots of $k_{obs}(1)$ and $k_{obs}(2)$ versus [NP] are shown in Figure S6, Supporting Information). Thus, although the two-exponential analysis was applied to kinetic traces that indicated dual reaction pathways, it allowed only a crude estimation of the selected kinetic parameters that characterize the reaction system (see text below). On the contrary, analysis of the kinetic traces according to a single-exponential model, although these resulted in much

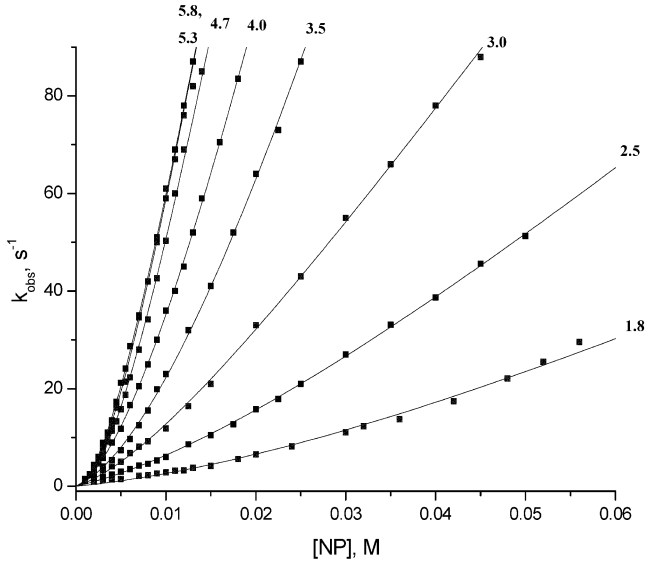

Figure 9. Plots of k_{obs} vs [NP] resulting from the one-exponential fit of kinetic traces at different pH (as indicated in the figure). [Cbl(II)] = 1×10^{-4} M, 25 °C.

less satisfactory mathematical fits (compare Figure S7, Supporting Information), did give consistent and reproducible results and enabled determination of kinetic and thermodynamic data which could not be obtained from the two-exponential model. Thus, both methods of analysis of the experimental data were applied in order to provide kinetic characterization of the reaction system.

Figure 9 presents the plots of the observed first-order rate constants versus [NP] obtained from the single-exponential fits of the kinetic traces in the pH range 1.8−6. Two noteworthy features of these plots are the nonlinear dependence of the observed rate constants on the [NP], and the marked dependence of the reaction rate on pH. The reactions considered to account for the observed kinetics involve a rapid preequilibrium which leads to the formation of the cyano-bridged precursor, followed by the rate-determining inner- and outer-sphere electron-transfer steps, as presented in Scheme 4. The suggested mechanism is consistent with the rate law described by eq 8

$$k_{obs} = k_{-5}[CN^-] + k_5\left\{\frac{K_2[NP]}{1 + K_2[NP]}\right\} + k_6\left\{\frac{K_2[NP]^2}{1 + K_2[NP]}\right\} \quad (8)$$

Due to the reversible nature of the inner-sphere electron-transfer path, it is essential to include the back reaction characterized by the rate constant k_{-5} in the overall reaction scheme. However, the influence of the reverse reaction path on the kinetics was meaningful only under nearly stoichiometric concentrations of the reactants (as described earlier), or in the presence of externally added cyanide. In the presence of the large excess of NP employed in the kinetic studies, its contribution was very small (as indicated by negligible intercepts in the plots presented in Figure 9), and thus the term $k_{-5}[CN^-]$ in eq 8 was neglected in the subsequent treatment of the data. To resolve the overall reaction that proceeds via parallel pathways with different mechanisms into the contribution of each pathway, the data presented in Figure 9 were fitted to eq 8 (solid lines in Figure 9). The thermodynamic and kinetic parameters obtained from the respective fits are summarized in Table 1.

On the basis of the results obtained from the one- and two-exponential analysis, we ascribe the fast and slow components to the outer- and inner-sphere electron transfer pathways, respectively. The contribution of the inner-sphere path, however, was small under the employed experimental conditions (particularly at pH > 4), such that the experimental points presented in Figure 9 mainly reflect the kinetics of outer-sphere electron transfer. Consequently, reliable values of k_5K_2 could only be determined from fits to eq 8 in the pH range 1.8−3.5. These values, however, compare relatively well with that estimated from the plots of $k_{obs}(2)$ versus [NP] obtained from the two-exponential analysis of the kinetic traces in the pH range 1.8−5, which are summarized in the third column of Table 1 (in this case, the k_5K_2 values correspond directly to the slopes of the plots of $k_{obs}(2)$ vs [NP] presented in Figure S6-b).

The k_6K_4 values characterizing the outer-sphere electron transfer between $\mathbf{1_p}$ and nitroprusside could be determined from the single-exponential fits in the pH range 1.8−6. The rate constants k_6 calculated from these values and from the equilibrium constants K_2 (determined as the third parameter from the fits of experimental data to eq 8), increase significantly on increasing pH. This effect could be directly correlated with pH, as shown in Figure 10.

The main conclusions emerging from these kinetic studies can be summarized as follows. Under pseudo-first-order conditions with respect to NP, the contribution from inner-sphere electron transfer to the observed redox process decreases on increasing pH, and becomes negligible at pH > 5. Such a reactivity trend is in line with the influence of pH on the thermodynamics of inner-sphere electron transfer described in the previous section. It can be expected that on increasing pH, the equilibrium characterized by the rate constants k_5 and k_{-5} (Scheme 4) gradually shifts to the left and thus competes less efficiently with outer-sphere electron transfer between $\mathbf{1_p}$ and NP. Despite the modest accuracy of the data characterizing the inner-sphere path, they do provide evidence that the *rate* of this process increases in the pH range 2−5. The apparent pK_a value of 3.3 determined from the pH profile constructed from the k_5K_2 values given in Table 1, (Figure S8, Supporting Information) is similar to that obtained for the rate constant k_6 that characterizes the outer-sphere reaction path. The observed pH dependences of the inner- and outer-sphere reactions can be reasonably attributed to the acid−base equilibrium presented in Scheme 5. Electrochemical measurements indicated that this equilibrium significantly influences the redox properties of the cobalt center in complex **1** (as described in more detail below). The pK_a value of 3.4 estimated for this process from the redox potential measurements is in close agreement with that obtained from the kinetic data. The observed ca. 100-fold acceleration of the outer-sphere electron-transfer process resulting from coordination of dimethylbenzimidazole to the cobalt center, compares well with that reported in the literature for the reduction of selected organic halides by Cbl(II).[39]

The K_2 values reported in Table 1, although considerably scattered, indicate an increase in the stability of the precursor complex at higher pH compared to that observed in acidic medium. This trend can be rationalized in terms of the higher

(38) (a) This value was determined at pH 7 using a competition technique[38b] in which N_3^- was employed as the competing nucleophile (b) Nome, F.; Fendler, J. H. *J. Chem. Soc., Dalton Trans.* **1976**, 1212.
(39) Blaser, H. U.; Halpern, J. *J. Am. Chem. Soc.* **1980**, *102*, 1684.

Table 1. Kinetic and Thermodynamic Parameters for the Inner- and Outer-Sphere Electron Transfer Reaction of Cbl(II) with NP

pH	k_5K_2,[a] $M^{-1}s^{-1}$	k_5K_2,[b] $M^{-1}s^{-1}$	k_6K_2,[a] $M^{-2}\,s^{-1}$	K_2,[a] M^{-1}	k_6,[c] $M^{-1}\,s^{-1}$
1.8	$(1.8 \pm 0.4) \times 10^2$	$(2.5 \pm 0.1) \times 10^2$	$(1.1 \pm 0.3) \times 10^4$	12 ± 6	$(9 \pm 5) \times 10^2$
2.5	$(4.3 \pm 0.4) \times 10^2$	$(4.7 \pm 0.3) \times 10^2$	$(3.5 \pm 0.7) \times 10^4$	22 ± 6	$(1.6 \pm 0.5) \times 10^3$
3.0	$(6.4 \pm 1.3) \times 10^2$	$(9.3 \pm 0.2) \times 10^2$	$(1.3 \pm 0.3) \times 10^5$	51 ± 12	$(2.5 \pm 0.8) \times 10^3$
3.4		$(16.7 \pm 1.4) \times 10^2$			
3.5	$(8.0 \pm 1.5) \times 10^2$		$(2.0 \pm 0.2) \times 10^5$	27 ± 4	$(7.4 \pm 1.3) \times 10^3$
4.0	*d*	$(23.4 \pm 0.7) \times 10^2$	$(4.4 \pm 0.4) \times 10^5$	50 ± 6	$(8.8 \pm 1.4) \times 10^3$
4.7	*d*		$(1.0 \pm 0.1) \times 10^6$	93 ± 18	$(1.1 \pm 2.6) \times 10^4$
5.0	*d*	$(27.3 \pm 2.9) \times 10^2$			
5.3	*d*	*e*	$(1.3 \pm 0.3) \times 10^6$	118 ± 34	$(1.1 \pm 0.4) \times 10^4$
5.8	*d*	*e*	$(1.4 \pm 0.1) \times 10^6$	126 ± 14	$(1.1 \pm 0.2) \times 10^4$

[a] Values determined from the fit of experimental data to eq 8. [b] Values determined from the two-exponential analysis of kinetic traces. [c] Calculated from the values of k_6K_2 and K_2 obtained from the fit of the experimental data to eq 8. [d] Reliable determination of the k_5K_2 parameter was not possible (error limits larger than the values obtained from the fit). [e] Inner-sphere electron-transfer not observed.

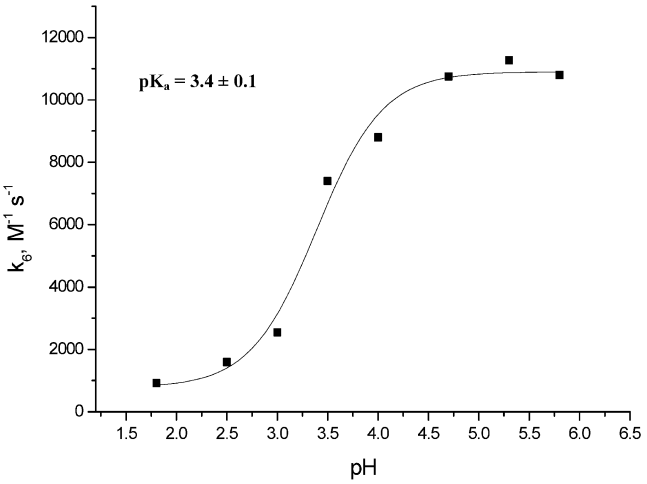

Figure 10. Plot of the second-order rate constant, k_6, versus pH for outer-sphere electron transfer between $[Cbl(II)-(\mu\text{-}NC)-Fe^{II}(CN)_4(NO^+)]^{2-}$ and $[Fe^{II}(CN)_5(NO^+)]^{2-}$.

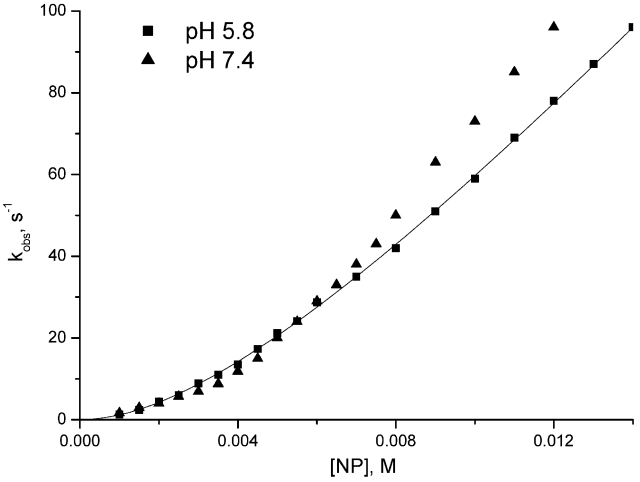

Figure 11. Comparison of the observed rate constants obtained from a single-exponential analysis of the absorbance/time plots at pH 5.8 and 7.4. Solid line represents the best fit of the data obtained at pH 5.8 to eq 8.

Scheme 5

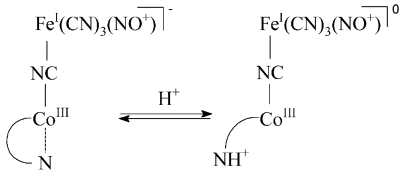

rate of NP coordination (i.e., larger k_2 value) to base-on reduced cobalamin (which involves binding of NP at the vacant coordination site) compared to base-off Cbl(II) (where substitution of a labile water molecule by nitroprusside must occur). The observed effect, however, is small. This observation is in agreement with previous findings on the coordination of NO^2 and selected organic radicals[40] to the base-on and base-off forms of Cbl(II). The equilibrium constant $K_4 = 126\ M^{-1}$ determined at pH 5.8 can be compared with that reported for the Cbl(II)CN adduct at basic pH (reaction 9)

$$Cbl(II) + CN^- \overset{K_7}{\rightleftharpoons} [Cbl(II)CN]^- \qquad K_7 = 2.4 \times 10^2\ M^{-1} \tag{9}$$

The lower equilibrium constant found in the present system is in line with the expected influence of a $[Fe^{II}(CN)_4(NO^+)]^-$ group coordinated to the cyanide carbon, which decreases the basicity of the adjacent nitrogen and hence weakens the Co−NC bond.

On increasing pH above 6, additional reactions which contributed to the absorbance change on a stopped-flow time scale could be observed. On the basis of the kinetic and spectroscopic measurements, these processes were identified as subsequent reactions involving the attack of CN^- on the primarily reaction products formed in the electron transfer step. This mainly includes formation of the α-cyano substituted species (reaction path **B** in Scheme 2) and, to a lesser extent, substitution of NP by CN^- in the initially formed complex **2** (reaction 7). Although these reactions occurred on a minute time scale in the pH range 5−6, at higher pH values their rate became close to that observed for the electron transfer steps. As the difference between the rate of electron transfer and the subsequent steps was still relatively large in the pH range 6−8, the interference from the latter processes observed under these pH conditions was quite small (although evident). Attempts were made to separate the interfering processes from the electron transfer steps by arbitrary choice of the time range in which the kinetic traces could be fitted with a single-exponential function. The resulting data presented in Figure 11 show that the observed rate constants do not differ significantly from that determined in the pH range 4.5−6. However, the data obtained in the pH range 6−8 could not be satisfactorily fitted to eq 8.

The one-exponential analysis could not be applied to the kinetic traces obtained at pH > 8, which gave good mathematical fits only for a model involving a three-exponential function (a typical kinetic trace obtained at pH 8.5 is presented in Figure

(40) Bakac, A.; Espenson, J. H. *Inorg. Chem.* **1989**, *28*, 4319.

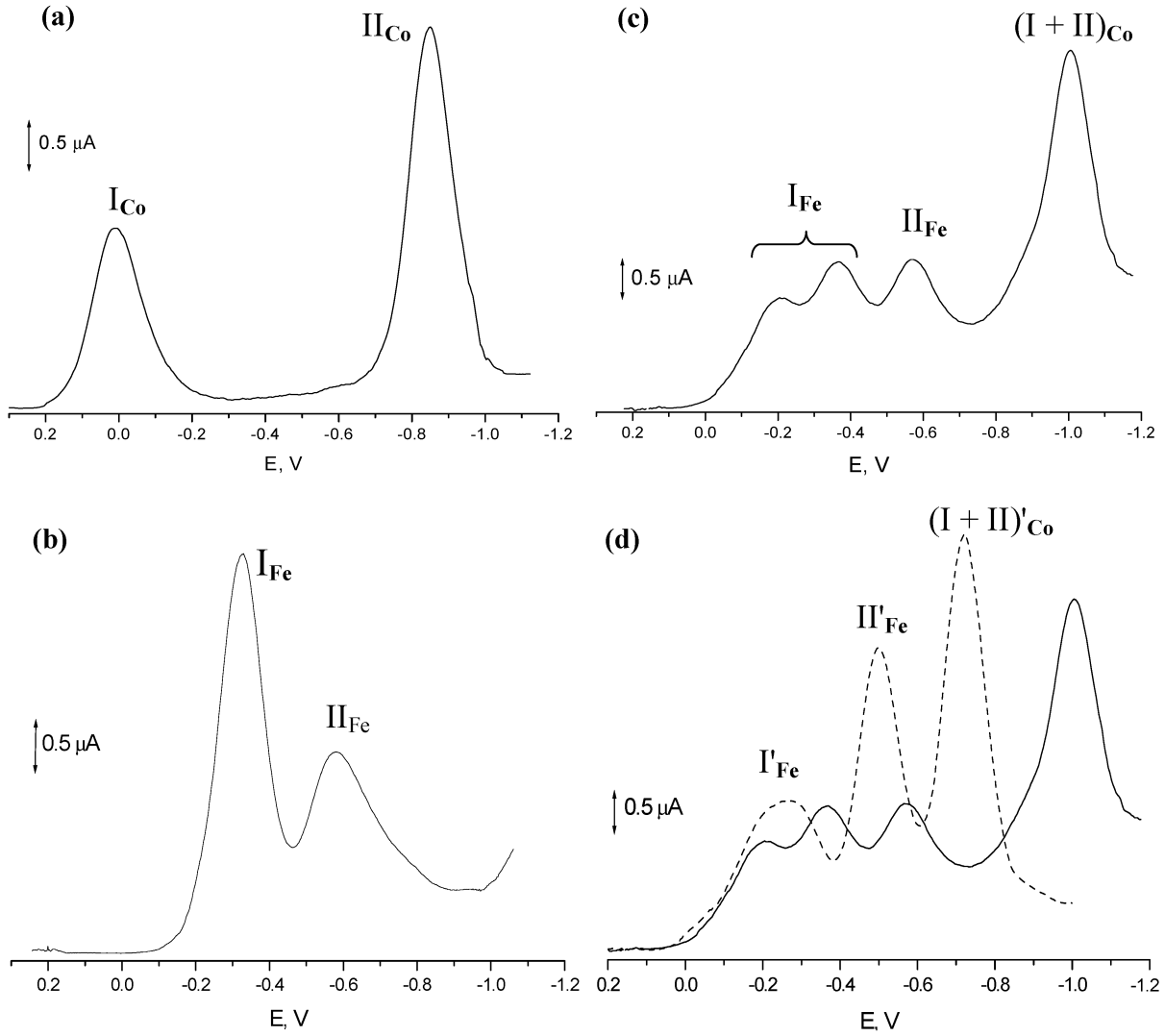

Figure 12. Differential pulse voltammograms of (a) aquacobalamin (1×10^{-3} M, pH 7.0), (b) NP (1×10^{-3} M, pH 7.4), (c) complex **2** formed by mixing of aquacobalamin (1×10^{-3} M) with NP (1×10^{-3} M) at pH 7.4, (d) comparison of differential pulse voltammograms recorded for complex **2** at pH = 7.4 (solid line) and 2.5 (dotted line). Symbols $\mathbf{I_{Co}}$, $\mathbf{II_{Co}}$, $\mathbf{I_{Fe}}$, and $\mathbf{II_{Fe}}$ denote peaks corresponding to the first and second reduction of the cobalt and iron center, respectively. $\mathbf{I'_{Co}}$, $\mathbf{II'_{Co}}$, $\mathbf{I'_{Fe}}$, and $\mathbf{II'_{Fe}}$ represent the corresponding peaks observed at low pH. Experimental conditions: DPV recorded in 0.1 M $NaClO_4$, pH = 7.4 and 2.5 adjusted with NaOH and $HClO_4$, respectively; scan rate 10 mV/s, pulse height 25 mV, step duration 0.2 s.

S9, Supporting Information). However, due to the fact that the observed processes occurred on a similar time scale (and in addition, small amplitudes attributable to the fastest and slowest component were observed), such analysis did not yield the rate constants which would enable reliable and reproducible analysis of the kinetic data. Nevertheless, it could be concluded qualitatively that the electron-transfer processes also in this case occurred on a time scale similar to that observed in the pH range 4.5−8.

Electrochemical Studies. Due to the fact that complex **1** formed in the reaction of reduced cobalamin with NP represents a one-electron reduced form of $[Cbl(III)-(\mu\text{-}NC)-Fe^{II}(CN)_4(NO^+)]^-$ (**2**), electrochemical techniques provide an opportunity to investigate the electronic properties of the metal centers in **1** and **2** and to compare them with that observed for the respective mononuclear species. Figures 12a-c show the differential pulse voltammograms of aquacobalamin, sodium nitroprusside and an equimolar mixture of both species (i.e., of complex **2**) at pH 7.4.[41] Reduction peaks of mononuclear cobalamin species corresponding to the Co^{III}/Co^{II} and Co^{II}/Co^{I} change in oxidation states are observed at ca. −0.01 and −0.86 V in the DPV of aquacobalamin, whereas those observed for the first and second reduction process in $[Fe^{II}(CN)_5(NO^+)]^{2-}$ appear at −0.36 and −0.58 V, respectively. The observed peaks correspond to the oxidation−reduction processes for which the potentials $E^1(Co^{III}/Co^{II}) = -0.02$ V, $E^2(Co^{II}/Co^{I}) = -0.83$V, $E^1(NP/NP^-)$ −0.34 V and $E^2(NP^-/NP^{2-})$ −0.58 V (vs Ag/AgCl) were reported in the literature.[18,34,42] Stepwise addition of NP to the aquacobalamin solution resulted in the disappearance of the Co^{III}/Co^{II} peak at −0.01 V (peak $\boldsymbol{I_{Co}}$ in Figure 12a). This was accompanied by a progressive broadening and a shift of the second reduction peak of cobalamin to a more negative potential. In a 1:1 molar mixture of the reactants, this peak is

(41) Differential pulse voltammetry offers a better resolution of poorly separated redox waves compared to cyclic voltammetry, and for that reason is mainly used in the discussion of the reductive processes observed for compex **2**. Cyclic voltammograms recorded in the corresponding potential range (compare Figure S10, Supporting Information) provided additional information on the reoxidation processes from reverse anodic scans. Detailed discussion of these data, however, is beyond the scope of the present study.

(42) Carapuça, H. M.; Simao, J. E. J.; Fogg, A. G. *J. Electroanal. Chem.* **1998**, *455*, 93, and references therein.

Scheme 6

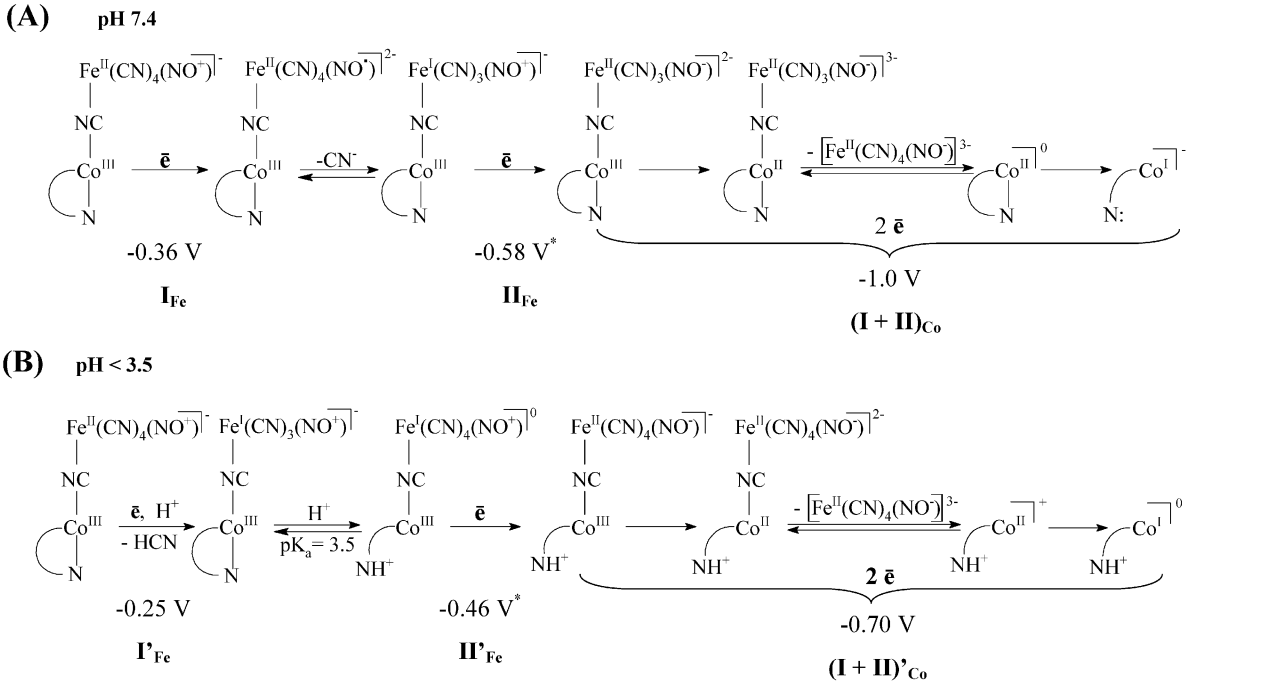

located at −1.0 V (peak $\mathbf{(I + II)_{Co}}$ in Figure 12c), and corresponds to an irreversible two-electron reduction wave with a maximum at ca. −1.04 V in the cyclic voltammogram recorded under the same experimental conditions (Figure S10-a, Supporting Information). In addition, three new peaks appear at −0.19, −0.36, and −0.58 V, the latter two located at potentials very similar to that characteristic for the first and second reduction of NP at pH 7.4. The same final differential pulse voltammogram resulted from the stepwise addition of one mole equivalent of aquacobalamin to the NP solution, where in this case splitting of the first reduction peak of NP into two peaks located at − 0.19 and − 0.36 V was accompanied by appearance of a new peak at −1.0 V.

We interpret the observed changes in the DPV of aquacobalamin in terms of a strong negative shift of the Co^{III}/Co^{II} redox potential to values close to that observed for a Co^{II}/Co^{I} reduction, as a result of substitution of a water molecule in $[Cbl(III)H_2O]^+$ by the bridging cyanide. Consequently, reduction of the cobalt center in **2** consists of the consecutive Co^{III}/Co^{II} and Co^{II}/Co^{I} electron transfer steps that occur at nearly the same potential, and is observed as a two-electron reduction wave at −1.04 V in the respective cyclic voltammogram (the irreversibility of this wave results from the occurrence of chemical reactions upon formation of the tetracoordinate Cbl(I), compare Scheme 6). Similar changes in the redox properties of aquacobalamin resulted from coordination of $[Fe(CN)_6]^{4-}$ to aquacobalamin (Figure S11, Supporting Information), where the $[Cbl(III)-(\mu\text{-}NC)-Fe^{II}(CN)_5]^{3-}$ complex is formed.[43] The observed large negative shift in the Co^{III}/Co^{II} redox potential is comparable with that resulting from coordination of CN^- to aquacobalamin (in this case, a very stable C-bonded Co^{III}-CN complex is formed).[10]

In contrast to the large effect on the redox properties of the cobalt center, the redox behavior of nitroprusside does not change significantly upon coordination to aquacobalamin. This is evidenced by the similar location of the peaks attributable to the iron center in the oligonuclear complex compared to that observed for $[Fe^{II}(CN)_5(NO^+)]^{2-}$. Splitting of the peak characteristic for the one-electron reduction of NP (peak $\mathbf{I_{Fe}}$ in Figure 12b) into two peaks centered at −0.19 and −0.36 V possibly reflects formation of cis and trans isomers of **2**, i.e., $[Cbl(III)-(\mu\text{-}NC_{ax})-Fe^{II}(CN_{ax})(CN_{eq})_3(NO_{eq}{}^+)]^-$ and $[Cbl(III)-(\mu\text{-}NC_{ax})-Fe^{II}(CN_{eq})_4(NO_{ax}{}^+)]^-$, respectively. Electrochemical reduction of the trans isomer is expected to result in its rapid and irreversible decomposition to cyanocobalamin and $[Fe^{I}(CN_{eq})_4(NO^+)]^{2-}$. A positive shift in the one-electron reduction potential of the iron center compared to that of free $[Fe(CN)_5NO]^{2-}$, as a result of a fast irreversible reaction following the electron-transfer step, can therefore be expected for the trans isomer. The cis isomer, however, does not undergo decomposition upon one-electron reduction, but is expected to release cyanide in a manner similar to that observed for free NP and, consequently, may exhibit a similar $E^1(NP/NP^-)$ value. Thus, it seems reasonable to ascribe the two peaks at −0.19 and −0.36 V to the trans- and cis-isomeric forms of **2**, respectively. The position of the second reduction potential of NP in the oligonuclear complex is very similar to that reported for $[Fe^{II}(CN)_5(NO^+)]^{2-}$. This suggests that similar mechanisms are operating in the second reduction process[44] for the bound and free nitroprusside.

Positive shifts in the potentials attributed to both metal centers in **2** were observed in the differential pulse voltammograms on

(43) Due to the absence of the redox-active NO ligand, cyclic and differential pulse voltammograms of $[Cbl(III)-(\mu\text{-}NC)-Fe^{II}(CN)_5]^{3-}$ are simpler than those obtained for $[Cbl(III)-(\mu\text{-}NC)-Fe^{II}(CN)_4(NO^+)]^{2-}$. This facilitates observation of changes in the electrochemical properties of the metal centres resulting from the formation of cyano-bridged species.

(44) Detailed electrochemical studies reported in the literature indicate that the nature of the reductive process occurring at the second reduction potential of NP is complicated and, in addition to a reversible one-electron reduction of $[Fe(CN)_4NO]^{2-}$, may involve its multielectron reduction, as well as comproportionation and adsorption phenomena.[42] However, for the sake of clarity, only the one-electron reduction of $[Fe(CN)_4NO]^{2-}$ (which is expected as the predominant process occurring at the second reduction potential under our conditions) is included in the discussion.

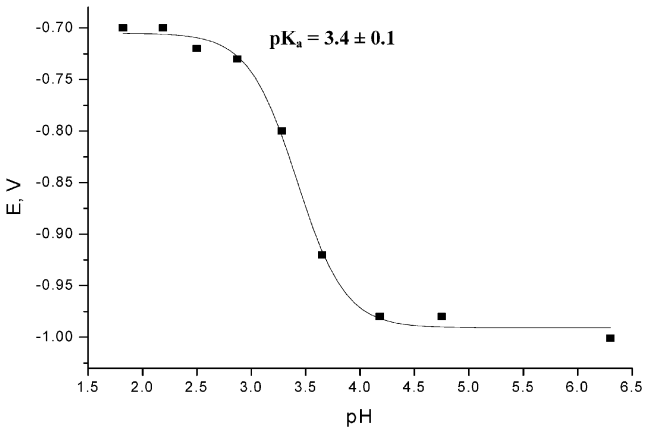

Figure 13. Plot of the potential observed for reduction of the cobalt center in complex **2** (peak $\mathbf{(I + II)_{Co}}$) versus pH.

lowering the pH from 6 to 2. The most significant changes involved the Co^{III}/Co^{I} potential, as evidenced by the gradual positive shift of the $\mathbf{(I + II)_{Co}}$ reduction peak from −1.0 to −0.7 V. This effect can be clearly seen from Figure 12d, which shows a comparison of the differential pulse voltammograms recorded at pH 7.4 and 2.5. The pH dependence of the Co^{III}/Co^{I} potential presented in Figure 13 clearly shows that the observed shift reflects the pH dependent process for which the $pK_a = 3.4$. This value is very close to that determined kinetically for the base-on/base-off equilibrium presented in Scheme 5, and provides confirmatory evidence for our earlier conclusions concerning the influence of this equilibrium on the rate of inner- and outer-sphere electron transfer.

The less marked positive shifts observedfor peaks $\mathbf{I_{Fe}}$ and $\mathbf{II_{Fe}}$ (from −0.36 to −0.25 V and from −0.58 to −0.46 V, respectively, compare Figure 12d) are similar to those reported for the monomeric $[Fe^{II}(CN)_5(NO^+)]^{2-}$ complex.[45] On the basis of literature data on the redox behavior of sodium nitroprusside,[34,42] as well as that reported for the reduction of cyanocobalamin (in which the cobalt center undergoes a simultaneous two-electron reduction similar to that observed in the system presently studied[10]), the differential pulse and cyclic voltammograms obtained at high (pH > 6) and low (pH < 3) pH, can be accounted for by the reaction sequences **A** and **B** (for high and low pH, respectively) presented in Scheme 6.

Cyclic and differential pulse voltammograms recorded for equimolar mixtures of reduced cobalamin and NP at pH 2 were similar to those obtained for complex **2** under similar experimental conditions, except that the peak at −0.19 V (attributed to the one-electron reduction of the Fe^{II} center in the trans isomer of **2)** was no longer observed. The similarity of cyclic and differential pulse voltammograms of complexes **1** and **2** provides confirmatory evidence that the stable product formed in the reaction of Cbl(II) with $[Fe^{II}(CN)_5(NO)^+]^{2-}$ in the low pH range is in fact a one-electron reduced form of **2**.

An important conclusion that arises from the above outlined observations is that coordination of $[Fe^{II}(CN)_5(NO^+)]^{2-}$ to cobalamin shifts the redox potential of the Co(III) center to more negative values than observed for the first (and second) reduction of bound NP. This means that the reaction of Cbl(II) with NP must involve formation of the $Co^{II}-(\mu\text{-NC})-Fe^{II}$ intermediate

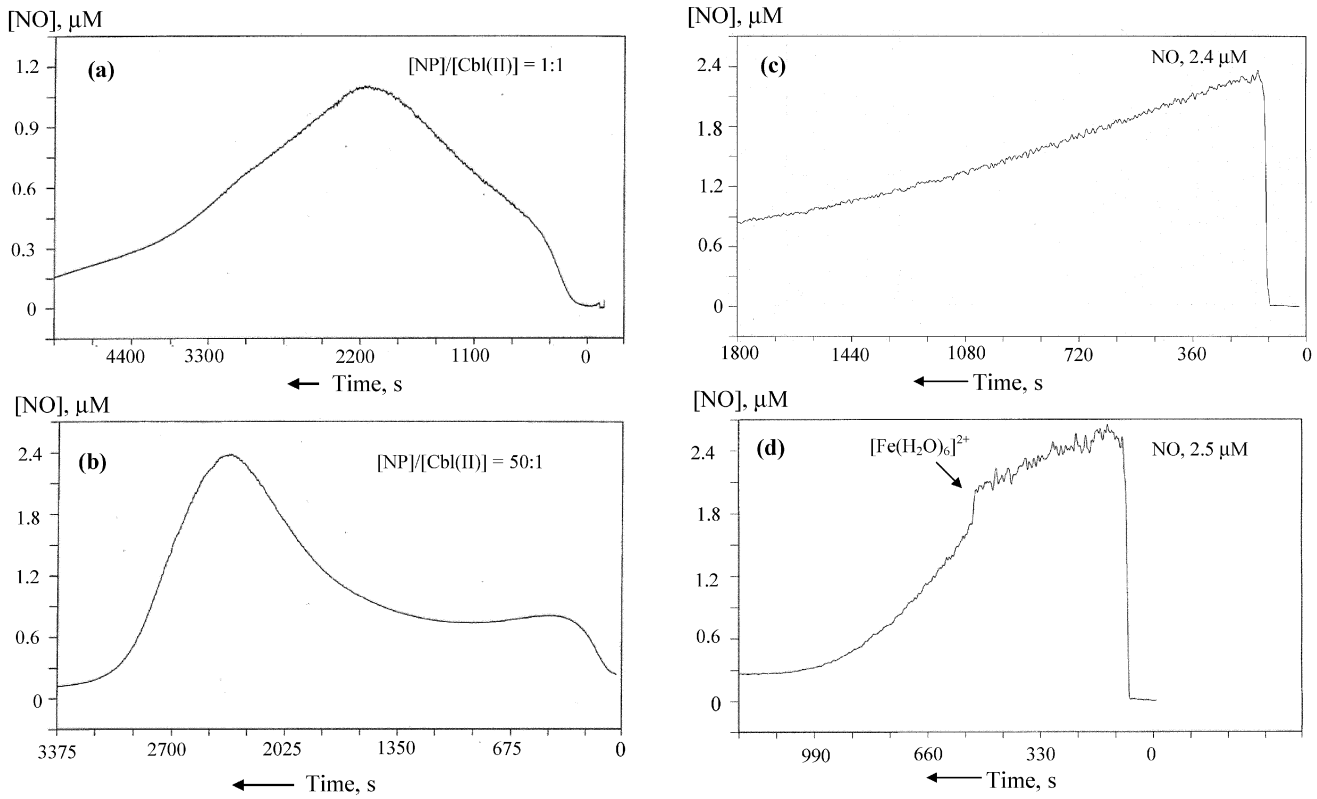

Figure 14. (a) Release of NO after addition of Cbl(II) (2×10^{-4} M) to NP solution (2×10^{-4} M) at pH 7.4 (0.1 M Tris-$HClO_4$), (b) as in (a), [NP] = 1×10^{-2} M, (c) decay of NO signal after addition of aqueous NO solution to deoxygenated buffer (pH 7.4), (d) as in (c), after addition of $[Fe(H_2O)_6]^{2+}$ (5×10^{-6} M).

Scheme 7

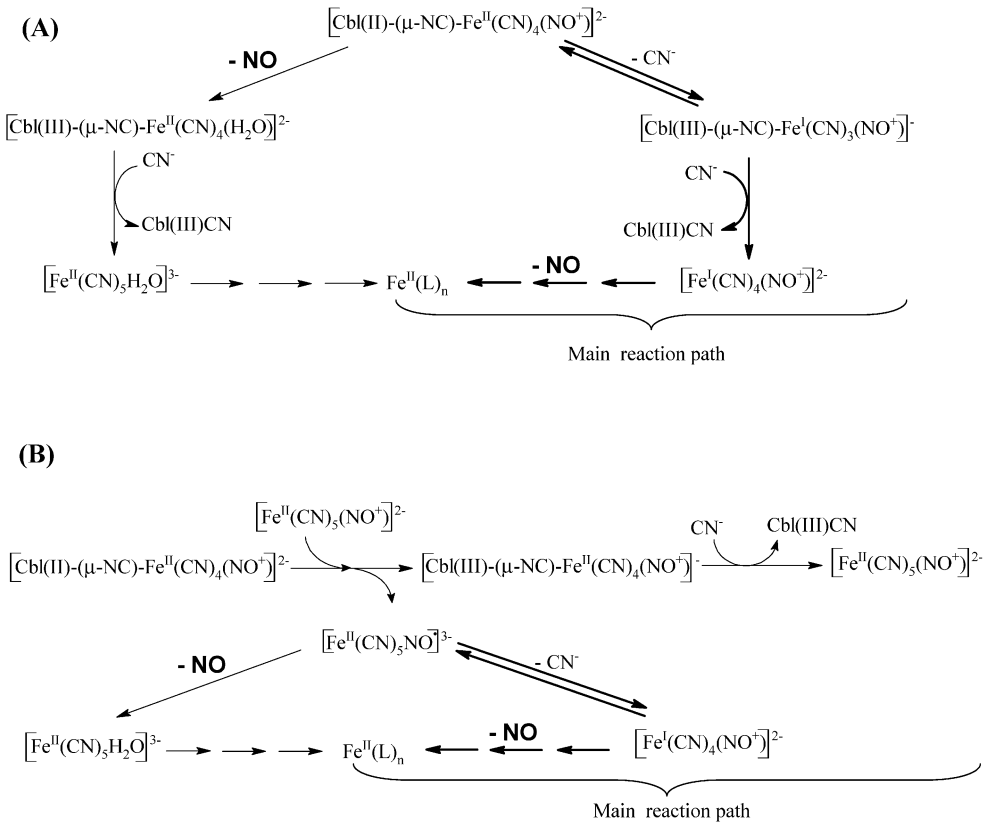

which undergoes electron transfer to form a highly thermodynamically favored $Co^{III}-(\mu\text{-NC})-Fe^{I}$ electronic isomer.

Release of NO at Physiological pH. Concentrations of NO released in the reaction of reduced cobalamin with NP at physiological pH was monitored with the use of an NO selective electrode at different Cbl(II) ($1 \times 10^{-4} - 5 \times 10^{-4}$ M) and NP concentrations ($1 \times 10^{-4} - 1 \times 10^{-2}$ M). A characteristic two-stage pattern of NO production observed after addition of Cbl(II) to a NP solution under oxygen-free conditions is shown in Figure 14, which reports the changes in [NO] after mixing Cbl(II) with an equimolar concentration (a) and with a large excess of NP (b) (i.e., under the conditions where the inner- and outer-sphere electron-transfer reactions are the dominating reaction paths, respectively). It becomes evident from these data that release of NO is rather slow, and the measured NO concentrations are low (the maximal observed NO concentrations $\approx$ 2% of that expected for stoichiometric release of NO from one-electron reduced NP). Correlation of the release of NO with the UV−vis spectral changes recorded under the same experimental conditions clearly indicated that the maximal increase in [NO] during the second, slower stage of NO release (observed ca. 50 min after mixing of the reactants, independent of the [NP] employed) occurs on a much longer time scale than the electron-transfer processes. The first stage of NO release could, however, be roughly correlated with the rate of electron transfer. In addition, experiments performed at different Cbl(II) and NP concentrations showed that the amount of NO released was proportional to the concentration of the reductant, but did not depend on the concentration of NP.

(45) No significant dependence on pH was observed for the peak ascribed to the one-electron reduction of the trans isomer of **2** in the studied pH range.

Our observation that NO is formed as a side product in the observed redox process is not unexpected in view of the literature data on the reactivity of nitroprusside, which is known to release CN^- rather than NO in the first reaction step following the one-electron reduction process.[24−27,42] However, release of NO may also occur as a side reaction that leads to stabilization of the reduced iron center, and may thus account for the observed small initial production of NO. This and other processes which are suggested to account for the observed patterns of NO production following the inner- and outer-sphere electron-transfer reactions are summarized in the reaction sequences **A** and **B** of Scheme 7. According to this scheme, the second stage of NO release that occurs on a long time scale results from slow decomposition of $[Fe^{I}(CN)_4(NO^+)]^{2-}$. It should be noted that due to the high affinity of the Co(III) center of cobalamin for CN^-, the electron transfer and subsequent substitution processes observed in the present system at pH 7.4 can be summarized by the overall reaction 10

$$\text{Cbl(II)} + [Fe^{II}(CN)_5(NO^+)]^{2-} \rightarrow \text{Cbl(III)CN} + [Fe^{I}(CN)_4(NO^+)]^{2-} \quad (10)$$

Thus, $[Fe^{I}(CN)_4(NO^+)]^{2-}$ is the main iron complex formed after both the inner- and outer-sphere electron-transfer reactions. Literature data provide evidence that this ion undergoes further decomposition to NO and various iron(II) complexes such as $[Fe(CN)_5H_2O]^{3-}$, $[Fe(CN)_6]^{4-}$, and $[Fe(H_2O)_6]^{2+}$, from which the latter two were suggested as the ultimate reaction products.[25,26] The NO concentrations measured in our experiments are, however, significantly lower than that expected for the stoichiometric release of NO from the $[Fe^{I}(CN)_4(NO^+)]^{2-}$ ion.

This observation can be accounted for by: (i) only partial decomposition of the tetracyanonitrosylferrate ion on the time scale of our measurements[46] (only scarce literature data could be found on the kinetics of this process); (ii) scavenging of NO by the iron(II) complexes formed during decomposition of $[Fe^{I}(CN)_4(NO^+)]^{2-}$. The latter possibility is supported by the characteristic rapid decay of NO following its maximum production. This feature was particularly evident in the experiments involving excess of NP, Figure 14b, and may result from reactions such as that given in (11), for which the equilibrium constant $K_{NO} = 1.2 \times 10^3\ M^{-1}$ (pH 5.0, 23 °C) has been reported[47]

$$[Fe(H_2O)_6]^{2+} + NO \rightleftarrows [Fe(H_2O)_5NO]^{2+} + H_2O \quad (11)$$

A similar effect was indeed observed upon addition of $[Fe(H_2O)_6]^{2+}$ to an aqueous NO solution, which resulted in a significantly faster decay of the NO signal compared to that observed for a blank NO solution of the same concentration, as reported in Figures 14c and d. Thus, binding of NO to Fe(II) complexes formed during decomposition of $[Fe^{I}(CN)_4NO]^{2-}$ may in fact lower the NO concentrations measured by the NO-electrode in the experiments involving Cbl(II) and NP.

Taking into account that the affinity of many physiological targets for NO is significantly higher than that of $[Fe(H_2O)_6]^{2+}$, formation of $[Fe(H_2O)_5NO]^{2+}$ should not affect the physiological activity of NP. Nevertheless, due to the fact that the NO^+ character of the nitrosyl ligand (and therefore its predisposition to undergo nucleophilic attack) is retained in $[Fe^{I}(CN)_4(NO^+)]^{2-}$,[7,27] interaction of one-electron reduced nitroprusside with cellular nucleophiles rather than spontaneous release of NO appears a more probable metabolic route leading to the observed pharmacological effects.

Conclusions

The results of this study clearly demonstrate that different reaction paths are followed by the reactants depending on the experimental conditions employed. The most important parameter in this respect is pH because this affects the rate and thermodynamics of the observed inner- and outer-sphere electron-transfer processes through the pH-dependent equilibria involving the precursor complex, $[Cbl(II)-(\mu\text{-}NC)-Fe^{II}(CN)_4(NO^+)]^{2-}$. These include (i) the release of a peripheral cyanide ligand from the coordinated iron complex, and (ii) dechelation of the DMBI base from the cobalt center. A strong influence of pH on the subsequent substitution processes leading to the formation of the final reaction products Cbl(III)CN and $[Fe^{I}(CN)_4(NO^+)]^{2-}$, reflects the competition between H^+ and the Co(III) center for the cyanide released during the electron-transfer step.

With respect to the possible influence of cobalamin on the physiological activity of NP, the following points should be addressed. The electrochemical results indicate that formation of $[Cbl(III)-(\mu\text{-}NC)-Fe^{II}(CN)_4(NO^+)]^-$ (**2**) does not significantly affect the redox properties of nitroprusside. Thus, biological processes involving reductive activation of nitroprusside to initiate the release of NO should not be significantly influenced by formation of **2** in vivo. Experimental results also indicated that substitution of NP in complex **2** by cyanide is highly thermodynamically favored. This result is in agreement with the significantly higher stability constant of Cbl(III)CN compared to that determined for complex **2**. Thus, although binding of NP to $[Cbl(III)H_2O]^+$ is kinetically faster than the corresponding reaction with CN^-, and in the presence of both CN^- and NP would prevail on a shorter time scale, the thermodynamically driven conversion of **2** to Cbl(III)CN and NP will occur on a longer time. Results obtained at physiological pH indicate that the one-electron reduction of nitroprusside in complex **2** leads to the release of CN^-, which at this pH effectively substitutes the $[Fe^{I}(CN)_4(NO^+)]^{2-}$ group in the cyano-bridged complex **1** to form Cbl(III)CN and free $[Fe^{I}(CN)_4(NO^+)]^{2-}$. The latter species, however, is expected to undergo the same metabolic transformations leading to donation of NO as that occurring after the one-electron reduction of free NP in vivo. It may, therefore, be concluded that as far as the results of the present study are concerned, binding of NP to cobalamin should neither significantly affect the NO-donating ability of NP, nor exclude cobalamin as an effective scavenger of cyanide released from metabolized NP.

Acknowledgment. Studies at UEN were supported by the Deutsche Forschungsgemeinschaft as part of SFB 583 "Redox-Active Metal Complexes: Control of Reactivity via Molecular Architecture". Studies at UJ were supported by the State Committee for Scientific Research, Poland, KBN (3T09A13518). M.W. gratefully acknowledges support from DAAD.

Supporting Information Available: Figures S1−S11 referred to in the text are available via the Internet at http://pubs.acs.org. See any current masthead page for ordering information and Web access instructions.

JA0210852

(46) Concentrations of nitric oxide were monitored for ca. 2 h after mixing of the reactants.
(47) Wanat, A.; Schneppensieper, T.; Stochel, G.; van Eldik, R.; Bill, E.; Wieghardt, K. *Inorg. Chem.* **2002**, *41*, 4.